University of California, Merced

Characterization and optimization of dielectric barrier discharge plasma for enhancing plant growth rate

A dissertation submitted in partial satisfaction of the requirements

for the degree Doctor of Philosophy

In

Mechanical Engineering

By

Edgar Perez-Lopez

Committee in charge:

Professor Venkattraman Ayyaswamy, Chair

Professor Reza Ehsani, Advisor

Professor Min Hwan Lee

Professor Gerardo Diaz

2023

The Dissertation of Edgar Perez-Lopez is approved, and is acceptable in quality and form for publication on microfilm and electronically:

_____

Venkattraman Ayyaswamy, Chair

_____

Reza Ehsani

_____

Min Hwan Lee

_____

Gerardo Diaz

University of California, Merced

2023

Contents

Dedication:

To my family, friends, and all others who were present throughout my academic and life journey.

Acknowledgement:

I would like to express my sincere gratitude to the members of my committee for their invaluable input and thought-provoking questions during the qualifying examination. Their perspectives and insights enabled me to broaden my understanding of my research and pursue additional goals.

I am deeply grateful to Dr. Venkattraman Ayyaswamy for offering me the opportunity and unwavering support to embark on this doctoral journey in the field of mechanical engineering. The past five years have been a period of tremendous growth for me, both academically and personally, and I am indebted to you for granting me the academic freedom to explore and excel. In addition, I'd like to thank all agencies that have funded my projects and education along the way including the California Energy Commission, the National Science Foundation, and the University of California, Merced.

Furthermore, I would like to extend my appreciation to all the professors with whom I had the privilege of collaborating, whether through research or teaching. The wealth of knowledge I have acquired as a result of my interactions with the faculty at the University of California Merced is beyond measure, and I am immensely thankful for the guidance and mentorship they have provided.

In conclusion, I am humbled and immensely grateful to everyone who has contributed to my academic and personal development during this transformative journey. Your support, encouragement, and expertise have been instrumental in shaping my growth as a researcher and an individual.

Curriculum Vita

August 2023

Education

Ph.D. Mechanical Engineering, University of California Merced, August 2023.

Dissertation: "Characterization of dielectric barrier discharge plasma for application in growth rate enhancement of plants."

B.S. Mechanical Engineering, University of California Merced, May 2018

Research experience

Graduate Research Assistant, University of California Merced, 08/2018-Summer 2023

Design and analyze low temperature dielectric barrier discharge plasma reactors for various applications including agriculture, dry gas reforming, and surface modification.

Teaching experience

Instructor of Record, **University of California Merced**, 05/2023-08/2023

Eng. 120 Fluid Mechanics

Instructor of Record, **California State University Fresno**,01/2023-05/2023

ME (Mechanical Engineering) 029 Engineering Mechanics (Statics and Dynamics)

Teaching Assistant, **University of California Merced**, 01/2022-05/2023

MSE 113 Materials Characterization

Instructor of Record, **University of California Merced**, 05/2022-08/2022

Eng. 120 Fluid Mechanics

Teaching Assistant, **University of California Merced**, 08/2021-12/2021

ME 138 Introduction to Computational Fluid Dynamics

Teaching Assistant, **University of California Merced**, 08/2020-12/2020

ME 136 Fundamentals of Aerodynamics

Teaching Assistant, **University of California Merced**, 08/2019-05/2021

Engr. 057 Statics and Dynamics

Publications

Journal Publications

Perez-Lopez, E., Gavrilova, L., Disla, J., Goodlad, M., Ngo, D., Seshappan, A., Sharmin, F., Cisneros, J., Kello, C. T., & Berhe, A. A. (2022). Ten simple rules for creating and sustaining antiracist graduate programs. *PLOS Computational Biology*, *18* (10), e1010516.

Buendia, J, **Perez-Lopez**, **E**., and Ayyaswamy, A. "System-level model and experiments for irrigation water alkalinity reduction and enrichment using an atmospheric pressure dielectric barrier discharge," *Water Research*, 144, 2018, pp. 728-739.

Journal Publications under review

Sehgal M., Gautam P., **Perez-Lopez E.**, Ahmed S., Banerjee S., "Micro plasma-base surface modification of soft biocompatible polymers towards the modification of surface properties for biomedical applications: surface characterization using topography and electrical impedance spectroscopy," MRS Advances, 2023.

Journal Publications in preparation

Perez-Lopez E., Nguyen K., Ayyaswamy V., Dielectric Barrier discharge atmospheric pressure nonequilibrium plasma jet combination configurations for irrigation water enrichment consideration.

Perez-Lopez E., Olszewski A., Ayyaswamy V., Application of a dielectric barrier discharge atmospheric pressure jet for growth rate enhancement of vegetables.

Conference Presentations/Posters

Perez-Lopez E., Seghal M., Gautam P., Manimaran M., Banerjee S., "Micro Plasma-based surface modification of biocompatible polymers and composites towards the modification of surface properties for biomedical applications", 152nd The Minerals, Metals, and Materials Society (TMS) Annual Meeting and Exhibition, 2023.

Gautam P., Sehgal M., **Perez-Lopez E**., Mizuno W., Nguyen T., Ayyaswamy V., Leal-Quiros E., Diaz G., Banerjee S., "Development of a smart water pre-treatment system for controlled environment agriculture using micro-plasma and AI machines," USA FIRA 2022, The California Agricultural Robotics and Technology Forum, 2022.

Perez-Lopez E., Ayyaswamy V., "Investigation of dielectric barrier discharge plasma jet for consideration for agriculture," 49th International Conference on Plasma Science, 2022.

Perez-Lopez E., Ayyaswamy V., "Irrigation water enrichment using atmospheric pressure dielectric barrier discharge," 72nd Gaseous Electronics Conference, 2019.

Awards

UC Merced Mechanical Engineering Outstanding Teaching Award	2022
NSF AGEP CA HSI Alliance Fellowship	2022
Graduate Dean's Advisory Council on Diversity Award	2021
Rose R. Ruiz Fellowship	2020
IME Becas Scholarship Award	2020
Miguel Velez Fellowship	2019

Professional Affiliations

The American Society of Mechanical Engineers

The American Physical Society

The Institute of Electrical and Electronics Engineers

Mentorship

Mentor, Undergraduate Research Opportunities Center, University of California, Merced, 2020, 2022, and 2023.

Mentor, Grad-Excel Peer Mentorship Program, University of California, Merced, 2022-2023.

Mentor, Competitive Edge Summer Bridge Program, University of California, Merced, 2019.

Service

President, Graduate Student Association, University of California, Merced, 2022-2023.

Undocumented Affairs Officer, Graduate Student Association, University of California, Merced, 2021-2022.

Graduate Student Representative, Graduate Council, University of California, Merced, 2021-2022.

Council Member, Graduate Dean's Advisory Council on Diversity, University of California, Merced, 2019-2022.

Abstract:

Characterization of dielectric barrier discharge plasma in food, water, and energy systems

A Ph.D. dissertation by: **Edgar Perez-Lopez**

Mechanical Engineering

University of California, Merced. 2023.

Committee Chair: Professor Reza Ehsani

Dielectric barrier discharges (DBDs) are self-sustaining electrical discharges in electrode configurations containing an insulating material in the discharge path that allows for a self-pulsing plasma operation and thus, formation of a nonthermal plasma at normal pressure. In agriculture, DBDs have been shown to increase nitrate ion concentration in water treatment experiments, while increased reactive oxygen and nitrogen species from the plasma chemistry allow for germination rate of seed to increase. Thus, the application of the DBD reactors is wide and it is a reason to continue studying further with different configuration to determine potential candidates for current and new applications.

To begin with, a general overview of introduce plasma and relevant parameters crucial to the studies is presented. Plasma ignition requires specific power to reach specific frequencies such as alternating current (AC) and direct current (DC).

Then, the first study characterizes three in-house DBD reactors to determine power dissipation, injection, and yield for further characterization. The results report an efficient rate of injection of nitrate and the specific configuration and parameters of the DBD necessary to attain relatively high efficiency.

Thereafter, a DBD configuration with highest efficiency with respect to nitrate ions and energy dissipation of plasma will be utilized to study the growth rate enhancement capabilities of plasma activated water on vegetable plants, while characterizing the plasma chemistry and electrical properties. Additionally, the water properties as a function of plasma treatment time, while providing a concluding remark on growth rate enhancement capability of such reactor.

Chapter 1
Introduction and Literature Review

1.1 Plasma, the fourth state of matter

Lightning, plasma cutters, plasmons, and sun wind are all examples plasma the fourth state of matter and was first defined by Langmuir as a description of the region of discharge not influenced by wall and/or electrodes. The transition of matter to plasma occurs by the heating of molecules to increases their energy and transform matter in the following sequence: solid, liquid, gas, and plasma. The gas to plasma transition starts with molecules in gas dissociating to form a gas of atoms, then as the temperature is increased further the gas of atoms becomes a gas of freely moving charged particles, electrons, and positive ions. The state of plasma can be characterized as a mixture of electrons, ions, and neutral particles moving in random directions making it electrically neutral and electrically conductive allowing it to surpass conductivities larger than those of metals such as gold and copper [1].

In addition, plasma can have temperatures and energy densities greater than those produced by ordinary chemical means. The energetic species produced in plasma can initiate chemical reactions that otherwise would be difficult or impossible with ordinary chemical mechanisms. The

generated energetic species include charge particles such as electrons, ions, and radicals; highly reactive neutral species, excited atomic states, reactive molecular fragments; different wavelength photons, and can also initiate physical changes in material surfaces. Plasma can be separated into two distinct groups; the first group approaches a state of local thermal equilibrium and is also called thermal plasma or high temperature plasma, whose electrons, ions, and neutrals are assumed to have the same temperature. Non thermal, cold plasma, or low temperature plasmas, have electrons whose temperature reaches 10,000K while other particles such as neutrals remain at the ambient temperature of the environment.

1.2 Low Temperature plasma applications

In low temperature plasmas, the momentum transfer between light electrons and heavy particles (ions and neutrals) is not efficient and the power applied to plasma favors electrons; therefore, the electron temperature (T_e) is much higher than that of ions (T_i) and neutrals (T_n). These plasmas can be generated by corona discharge, glow discharge, arc discharge, capacitively coupled discharges, inductively coupled discharge, wave heated plasma, etc. [2]. The applications of low temperature plasmas have expanded to cover many fields including environmental engineering, aeronautics and aerospace engineering, biomedicine, textile technology, and analytical

chemistry. In industry, CO_2 dissociation in nonequilibrium plasmas under supersonic flow conditions can have shown to increase CO production selectively when the vibrational temperature reaches ~4000K and the translational temperature is only around 300K. This plasma process is also being researched for fuel production in mars, where the atmosphere primarily consists of CO_2.

In addition to industrial applications, low temperature plasma has been used as a technology for abating low volatile organic compound (VOC) emissions and other industrial exhaust products. The treatment of low temperature nonequilibrium plasmas has been effective in treating a range of emissions including aliphatic hydrocarbons; chlorofluorocarbons; methyl compounds, sulfur, and nitrogen oxides. The plasma produced in this nonequilibrium plasma process is dominated by electric energy which in turn produce energetic electrons. These electrons produce excited species, free radicals, ions, as well as additional electrons through the electron impact dissociation, excitation, and ionization of the background molecules. Ultimately, the active species oxidize, reduce, or decompose the pollutant molecules.

Low temperature plasmas have been applied in material processing, for example, in the coating industry the plasma's large enthalpy content, high temperatures, and large deposition rates are advantageous for increases

throughputs. The plasma typically powered by an RF power supply provide the ability to mix and blend materials that are otherwise incompatible. This type of plasma process Is preferred for the manufacturing of electronic components and wear- and heat-resistant coatings. Furthermore, plasma treatments of polyester have also been demonstrated to promote adhesion of gelatin-containing layers used in production photographic film. For the latter, low frequency, capacitively coupled nitrogen plasmas have proven particularly effective.

1.3 Plasma discharges and configurations

Streamer Corona Discharges

A corona discharge can be physically described as miniature lightning that forms at points and wires having high electrical potential with respect to the environment, creating a crown like shape with a faint glow. An example is a corona rising around high-voltage wires of an electrical power transmission line resulting in a loss of electrical energy. Corona discharges have many practical applications such as dust collection with electrical precipitators, atmospheric pressure non-thermal plasma surface treatment of polymers, cleaning of exhausted gases, etc. It can be described as a low-current discharge caused by partial breakdown of gas gap with strongly homogenous electric field. The inhomogeneous electric field can be formed by

having at least one of the electrodes sharpened with a radius of curvature of far less than the length of the inter-electrode gap. Figure (1) is a schematic of different dc coronas in a static ambient air at atmospheric pressure in pin-to-plate gaps under positive and negative polarities of high-voltage stressed pin electrode, the discharge current increases from left to right. The furthest right coronas in both negative and positive occur when the voltage levels are too high causing a corona-spark transition. Other electrode configurations exist that are also capable of generating a corona discharge, they include multi-wire-to-plane, wire-to-pipe, wire-to-plane, or wire between two planes, coaxial wire-cylinder and so on [3].

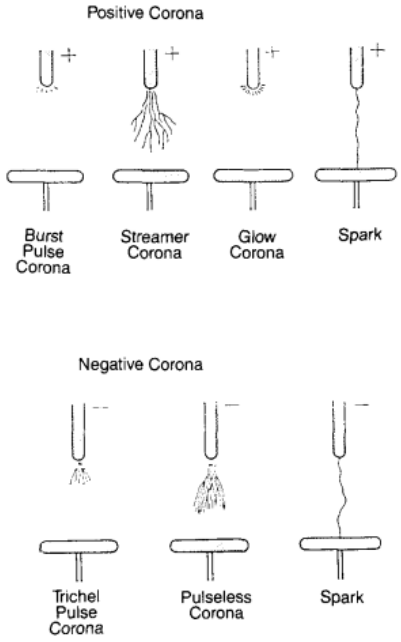

Figure 1. Schematic view of types of corona discharges (from Chang et al 1991)

AC Corona Discharges

Varying the voltages applied across a corona gap introduce new attributes in the physics of the discharge. For starters, the low mobility of the charge carriers in air and low concentration of ions in the bulk, the displacement current can be a marked or even dominant component of the total corona current at relatively low frequencies of the power supply in use. In centimeter gaps of pin-plane coronas, the number density of the ion space charge may range from $n_i = (2x10^9) - (2x10^{10})$ cm^{-3} depending on the magnitude of the corona current, thus the displacement current must be considered in ac coronas at frequencies of applied voltages from $f \geq 10^2\text{-}10^3$ Hz. In addition to this, the ac corona can act as a bipolar DC corona between two wires or sharpened pins at a certain frequency. This causes the drift region of an ac corona to be filled with ions of the opposite sign that tend to diminish the resultant space charge in the drift region and that are subjected to volume recombination. In general, the alternating electric field applied to a typical corona set up can cause the plasma to behave differently as a function of frequency and alternating electric field amplitude, making AC corona discharges relevant for many applications.

Dielectric Barrier discharge

The Dielectric Barrier Discharge (DBD) can be described as two metal electrodes separated by a gap that ranges from 0.1 mm to several centimeters and one or both electrodes are covered with a dielectric material. These are well known configurations that have been studied and applied in various fields and applications. One of the benefits of using configurations such as these is the ability to avoid corona-to-spark transitions at high voltages. Additionally, operation of DBDs can occur in strongly non-equilibrium conditions at atmospheric pressure and high-power levels, without the use of sophisticated power supplies. The dielectric barrier materials include glass, quartz, ceramics, and other low dielectric loss and high breakdown strength. Figure (2) includes some common DBD configurations that have been studied thoroughly in both DC and AC type of power supplies.

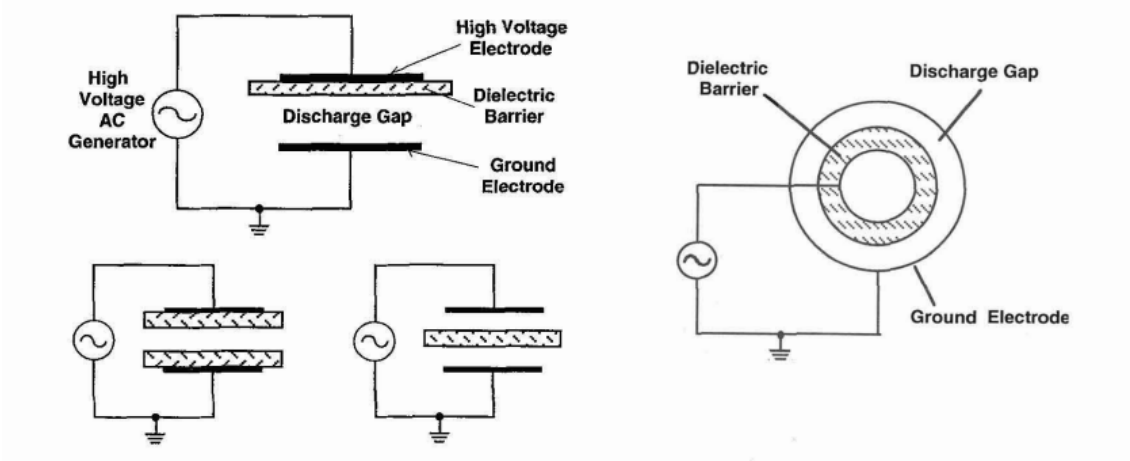

Figure 2. Common configurations for dielectric-barrier discharge. (From Kogelschatz et al 1997)

In an AC powered circuit, a DBD with a gap of a few millimeters would require a frequency between 500 Hz to 500 kHz and a voltage of about 10kV. The discharge in the gap occurs in several individual tiny breakdown channels called microdischarges. Physically, these microdischarges can be described as streamers that are self-organized considering charge accumulation on the dielectric surface. This leads to a physical "footprint" from the microdischarge that can be seen on dielectric surfaces or electrodes depending on the voltage and frequency of the power supply. The properties for microdischarges are independent of the external circuit and depend solely on the gas composition, pressure, and the electrode configuration. In a typical DBD, increasing the power input increases the number of microdischarges generated per unit time, which simplifies scaling of the dielectric barrier discharge. Microdischarges can also form at a point where a streamer has

struck and charge has been accumulated, these microdischarges or streamer families may result into an organized structure if power input is high enough [1].

Dissipation Power of DBDs

Parameters such as current and power dissipation in most DBDs at atmospheric pressure generally occur in many short-lived microdischarges that can be described by average quantities. In a DBD configuration where an AC voltage is applied there exists periods of discharge activity, which occurs when the voltage in the gap is high enough to initiate breakdown and maintain a discharge and pauses in between when the gap voltage is below the breakdown voltage value. Power estimations of the discharge periods has been extensively reviewed by. Two most used methods of calculating power in a DBD discharge (1) are the current and voltage waveform-based method and the Lissajous curve approach (2) which can be derived using a variation of Manley's analytical approach [4].

$$P = \frac{1}{T}\int UIdt \quad (1)$$

$$P = \frac{1}{T}\int UIdt = \frac{C}{T}\int U\frac{dU}{dt}dt = fC\oint UdU \quad = FCS \quad (2)$$

The measured voltage and current can be difficult to implement due to the heavy distortion of the current waveform and the necessity to include all filamentary discharge in a single discharge period. Thus, a high bandwidth current probe, high voltage probe, and a high frequency digital oscilloscope are necessary to obtain data and calculate the dissipated power which can lead to a high price for calculating dissipated power. Additionally, attention must be paid for the proper span of integration to integrate full period of supply waveforms. Lissajous method on the other hand, uses an external capacitor connected in series with the DBD configuration whose voltage and in turn energy can then be established based on the capacitance and voltage reading taken from the oscilloscope allowing for power calculation with only having a high voltage probe as opposed to having an additional current probe. A schematic of the measurement set up equivalent circuit and resulting oscilloscope Lissajous curve are presented in Figure (3).

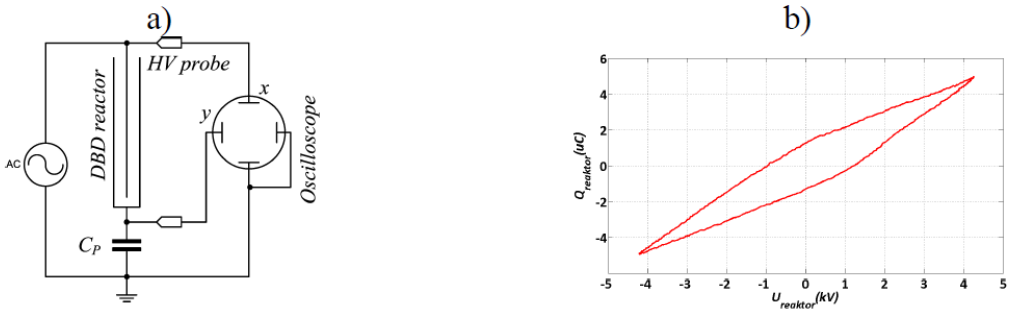

Figure 3. Lissajous curve a) measurement set-up b) exemplary Lissajous curve. (Taken from Holub M. 2012)

The oscilloscope is connected in series with both voltage probes and set in X-Y mode as opposed to the waveform method which utilizes the Y-T configuration to obtain the period and the magnitude of both the discharge current and the amplitude of the applied electric field.

Atmospheric Pressure Nonequilibrium Plasma Jet (APNP-J)

In typical nonequilibrium plasma at atmospheric pressure the electron temperature is much higher than that of the heavier molecules. This temperature increase causes the collision frequency between them to be high causing the electrons to lose energy in a short period of time making it difficult for the plasma to be sustained under atmospheric conditions. Additionally, electronegative gases such as O_2 and SF_6 can absorb electrons by the gas in a time scale of tens of nanoseconds or less, further complicating the ignition process for such plasma [2]. The same type issues occur during

the ignition process of atmospheric pressure nonequilibrium plasma jets (APNP-Js), where high electron-heavy particles' collision frequency and low electric field make it difficult to ignite. Noble gases are generally used to operate the plasma jets as their breakdown voltage allows for ease of ignition. These noble gas reactors can be classified into four categories, dielectric-free electrode (DFE) jets, dielectric barrier discharge (DBD) jets, DBD-like jets, and single electrode (SE) jets.

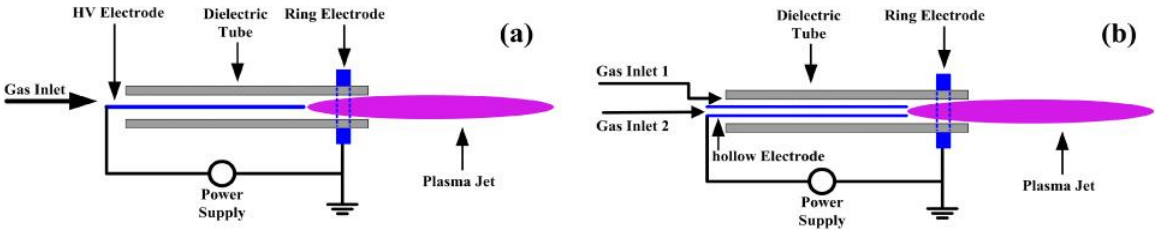

Figure 4. Schematic of DBD-like plasma jets. a) solid needle electrode with dielectric tube DBD-like plasma jet; (b) capillary tube inside dielectric tube DBD-like plasma jet

Figure 4(a) uses a needle electrode with a dielectric tube and a ring electrode at the exit of the tube, 4(b) replaces the needle shaped electrode with a capillary tube, but the ring remains present. Replacing the needle like electrode and adding and additional inlet to the reactor allows for plasma ignition of a noble gas in inlet 2 and some reactive gas such as O_2 and has been found to create a much longer plasma plume. Such reactors can be ignited using a kilohertz AC power supply, by RF power, or pulsed DC power. The capillary tube design served as motivation to development of the reactor

in question for the study and its preliminary characteristics are included in the study.

Typical operating parameters when considering plasma jets include the working gas, dissipated power, driven voltage, gas flow rate, and electrode configuration. Each configuration presented in Figure 4 work under specific condition and may exhibit distinct characterizations and can be used for various applications. An attractive feature of non-equilibrium plasma jets, aside from the various applications they can used for is their ability to achieve energy-intensive and effective gas phase chemistry without the needs for elevated gas temperatures. Ignition of plasma jets based on configurations can be achieves in two ways, the first is cross-field jet whose electric field is perpendicular to its flow field. The other is linear-field jet ignition with the electric field parallel to its flow field [5]. Plasma jet electrical excitation and sustainability of discharge plasma has been explored with direct current (DC), alternating current (AC), radio frequency (RF), microwave (MW) and pulsed power. While several plasma jets have been developed the past decades, there are several plasma jets that are yet to be reviewed and discussed, with the addition of a potential combination of other reactor configurations.

Alternating current (AC) plasma jets

Plasma jets under the alternating current (AC) power regime have been studied thoroughly as either DBD plasma jets or DBD-like plasma jets [6-8]. The plasma discharge can be characterized as a glow-like mode. While the plasma may seem homogenous in nature, it is in fact non-homogenous bullet-like discharge volume that was imaged utilizing fast imaging techniques. Orientation of the high voltage to ground electrode was found to be crucial to obtain specific plasma behavior, when switch the glow would vary depending on both gas flow and the connection.

In addition to this bullet like behavior exhibited in previous studies, there are operating modes that are specific to each reactor that can be obtained that depend on specific configuration. Three distinct operating modes including chaotic mode, bullet mode, and the continuous mode were observed in previous devices [9]. Increasing the dissipated power after plasma ignition allowed the plasma jet to evolve through these three modes of distinct differences and abrupt mode transition.

1.4 Plasma Chemistry and Plasma Physics

Electron impact reactions

Low temperature plasmas can be characterized by the energy channeled into the electron component of the plasma and/or vibrational non-equilibrium of the polyatomic species. The temperature of electrons in non-thermal plasmas far exceeds that of the ions and neutral species, whose translational temperature are close to equal and typically between room temperature and a few times the room temperature. Thus, nonthermal plasmas are a viable candidate in developing environments where very high energetic chemical processes can occur at low temperatures. The characterization of properties from nonthermal plasmas can be determined by using the collisions between plasma electrons and plasma constituents. The mean energy of the plasma electron being high make electron collisions important, as well as ionizing collisions, and, in molecular plasmas, dissociative electron collisions are of relevance. There are two ways that ionization collisions determine the charge carrier production, the first is by direct ionization of ground state atoms and/or molecules in the plasma and the second is stepwise ionization if an atom /molecule through intermediate excited states. The high number density of ground state atom/molecules during ionization requires a minimum energy above 10 eV for most species.

Electron impact dictates the chemical reactions in an air plasma with N_2 and O_2 being the main air plasma constituents. (R3-R11) are reactions for electro-driven processes for N_2 and O_2 (X) where the asterisk denotes either an excited state or a metastable. The last two reactions are only applicable to O_2 as it is electro negative and N_2 is not. The third body in R11 is required to satisfy energy and momentum conservation simultaneously.

$$e^- + X_2 \rightarrow X_2^* + e^- \quad (R3)$$

$$e^- + X_2 \rightarrow X + X + e^- \quad (R4)$$

$$e^- + X_2 \rightarrow X^* + X + e^- \quad (R5)$$

$$e^- + X_2 \rightarrow X_2^+ + 2e^- \quad (R6)$$

$$e^- + X_2 \rightarrow X_2^{+*} + 2e^- \quad (R7)$$

$$e^- + X_2 \rightarrow X^+ + X + 2e^- \quad (R8)$$

$$e^- + X_2 \rightarrow X^+ + X^* + 2e^- \quad (R9)$$

$$e^- + X_2 \rightarrow X^- + X \quad (R10)$$

$$e^- + X_2 + M \rightarrow X_2 + M \quad (R11)$$

The neutral chemistry and ion chemistry are connected through ion recombination in the gas phase as well as dissociative and associative ionization processes. The number of reactions for dry air is large to include and does not follow the structure of the current study, instead the example should be taken into consideration as a guide to understanding the types of processes occurring in the plasma [5-7].

Neutral chemistry in air plasmas

Air plasma ignition contains specific neutral species which is connected to ion chemistry through ion recombination processes in the gas phase or at the surface as well as dissociative and associative ionization processes. Important reactions to consider involve oxygen and nitrogen atoms and molecules, ozone, and NO_x reaction products. Table 1.1 summarizes important low-lying, long lived energy levels of the neutral species (N_2, O_2, N, and O) relevant to neutral chemistry in air plasmas in terms of the energy required for their formation via electron collisions [10-11].

Table 1.1 Low-Lying metastable states of N_2, O_2, N, and O (Radzig and Smirnov 1985)

Species	State	Energy (cm^{-1})	Energy (eV)
N_2	$A^3\sum_u^+$	50203.6	6.22
N_2	$B^3\Pi_g$	59618.7	7.39
N_2	$a'^1\sum_u^-$	69152.7	8.57
N_2	$C^3\Pi_u$	89136.9	11.05
O_2	$a^1\Delta_g$	7928.1	0.98
O_2	$b^1\sum_g^+$	13195	1.64
N	$^2D_{5/2}^0$	19224.5	2.384
N	$^2D_{3/2}^0$	19233.2	2.385
N	$^2P_{1/2}^0$	28839.9	3.576
O	$^1D_2$	15867.9	1.967
O	$^1S_0$	33792.6	4.190

In addition to processes in the gas-phase, heterogeneous processes such as surface interactions should also be considered. Aside from the reactions presented above, deactivation reactions of excited particles as well as recombination processes of atomic species and chemical reactions are important. The reaction probability for a given process depends on the surface material and the state of the surface in terms of its purity and

temperature. For processes at atmospheric pressure these processes are less important than those at lower pressures [12].

Plasma Spectroscopy

Atomic spectroscopy deals with primarily with wavelengths of spectral lines and is actively studied to establish energy-level structure of complicated atoms and highly ionized ions. The intensity of the lines can be utilized for determining the ionization stage of the ions emitting the line and the strength of the transition. Plasma spectroscopy deals with variable characteristics of the radiation emitted from the plasma in relation to the plasma itself, which is regarded as an environment of the atoms and ions emitting the radiation. The electromagnetic radiation emitted from the plasma is reflected in a series of mirrors and captured to create a spectrum of the radiation emitted which can provide information about the chemical species in the plasma [13].

In addition to obtaining information on the species of the plasma, one can obtain temperatures relating to electrons and molecules. The electron temperature, for example, can be obtained from line emission if the population densities of the upper levels of two lines are in partial local thermodynamic equilibrium (PLTE), where the upper levels of the species population can still be described by the Boltzmann distribution and connected to the ground state density of the next ionization stage.

If the lines of emission are in PLTE, the ratio of emission coefficients of two lines λ_{pq} and $\lambda_{p'q'}$ is given by

$$\frac{\varepsilon_z(p \to q)}{\varepsilon_z(p' \to q')} = \frac{\lambda_{p'q'}}{\lambda_{pq}} \frac{A_z(p \to q)}{A_z(p' \to q')} \frac{g_z(p)}{g_z(p')} \exp\left[\frac{E_z(p) - E_z(p')}{k_B T_e}\right] (3)$$

It is a sole function of the electron temperature T_e and to make the best use of the equation the lines selected should have a large energy separation of the upper levels. The more lines that are analyzed the higher the accuracy of the estimation. The logarithm of the number densities divided by the statistical weight should be plotted versus the energy $E_z(p)$ of the levels: such a plot is called a Boltzmann plot, a straight line with a slope of $k_B T_e$.

Furthermore, the population densities of the rotational and vibrational levels of electronically excited states of molecules obtained from line emission are usually characterized by rotational and vibrational temperatures, which are deduced by fitting a Boltzmann distribution. Both vibrational and rotational temperature can differ strongly from the electron temperature in plasmas where the population of these molecular states is governed by processes other than electron collisions [14].

1.5 Applications in food, energy, and water systems

Plasma Agriculture

Plasma agriculture began with the use of low-pressure plasma systems for the treatment of seeds but set ups that require low pressure generally require a more complicated and expensive set up. Non-thermal, atmospheric pressure plasma sources have allowed for improvements in the field, such as inline batch processing and the treatment of irrigation water. The main driving force in inducing seed growth in both low and atmospheric pressure was found to be the reactive oxygen and nitrogen species (RONS). Furthermore, nonthermal plasmas are a possible candidate for NO_3^- and NH_3 production through oxidation and reduction of N_2 after its dissociation.

Direct treatment of seeds by with plasma have been shown increased germination rate, increase root length, and enhanced growth of the seedlings [9,15]. In addition to the plant growth, plasma treatment of seeds has also been shown to help in disinfection through the ROS at the seed surface [16-18]. ROS have been shown to reduce pathogen loads and protect seeds from disease during germination at conditions that optimize growth of fungus or bacteria. Plasma treated water (PTW) also plays a role in the seed germination phase depending on the type of water used (DI, tap water, or distilled water) and the type of plasma used for treatment. Combination of plasma treatment and plasma irrigation has been considered and reviewed in

[19] that entails details of how significant process of plasma is to the seed germination and plant growth.

Energy efficiency of plasma-based processes.

There are several factors such as climate change, environmental pollution control, and resource utilization efficiency, as well as food security, sustainable agriculture, and water supply that society face today. There is a need across academic fields, technologies, and disciplines that is needed to generate ideas to meet several of these challenges. Plasma is considered as an inherently environment technology [112].

Plasma-based technologies for gas cleaning, for example, began with the development of electrostatic precipitators. These precipitators utilize corona discharges for the removal of dust from flue gases by means of physical mechanisms, namely electrostatic charging, ion migration, and electrohydrodynamic effects [113]. They enable high efficiency treatment and collection efficiency (99.9%) of large volumetric flows with lower pressure drops than alternative technologies such as cyclones or bag filters [114].

The degradation of chemical pollutants in gas streams as well as the removal of particulate matter such as soot and aerosols are possible with nonthermal plasmas. Research in the removal of nitrogen oxides (NO_x) and sulfur oxides (SO_x) from flue gases exiting combustion processes and of volatile organic compounds (VOCs) from off gases in manufacturing processes

[115]. The degradation of chemical compounds by nonthermal plasma is based on the collision of the pollutant molecules with free radicals and ions generated by the plasma. If oxygen and/or water vapor are significant constituents of the gas, the oxidizing reactions are dominant. For example, when treating NO_x, it results in higher oxides like N_2O_5, and in the presence of water molecules can lead to acids. Temperature, humidity, and chemical composition are main factors that affect the efficacy and selectivity of this chemical process.

Plasma reactors, such as DBDs, have also been utilized in water treatment and analyzed for their relative energy efficiency with respect to other thermal and nonthermal reactors alike. Complexity of the reactor geometry and power are contributing factors to the chemistry produced within the plasma. For example, a low temperature nonequilibrium discharge under ambient pressure may result in less species of interest than that of a reactor under low pressure and higher power input such as microwave.

1.6 Present fertilizer processes and energy consumption

The Haber-Bosch Process

During the early 20th century Fritz Haber and Carl Bosch developed the Habber-Bosch process which is a crucial industrial method for synthesizing ammonia (NH_3) from nitrogen gas (N_2) and hydrogen gas (H_2).

This process revolutionized global agriculture by enabling the production of synthetic nitrogen fertilizers on a large scale.

The method extracts nitrogen gas from air using methods such as fractional distillation or selective adsorption and air is compressed and cooled to separate nitrogen and other gases. Through steam reforming of natural gases hydrogen gas (H_2) can be obtained, where natural gas reacts with steam (H_2O) at high temperature and pressure to produce hydrogen gas and carbon dioxide. A ratio of nitrogen gas and hydrogen (typically 3:1) are introduced into a reactor vessel. In the reactor an iron-based catalyst along with other elements like aluminum or potassium are introduced to facilitate the breaking of the triple bond that holds the nitrogen molecule together and form ammonia (NH_3). The reaction takes place at a high temperature of approximately 400-500^{o}C and high pressure ranging between 150 to 300 atm, which favors the formation of ammonia, but requires significant energy input. Lastly, the reaction mixture, which now contains ammonia, unreacted nitrogen, and hydrogen gas, is cooled to condense the ammonia gas into a liquid state [116-118]. Thus, providing a reliable, but costly method to introducing nutrient rich fertilization for agricultural applications.

Acidification

In addition to the nutrients required for plants to grow efficiently, the soil pH also plays a crucial part during plant growth. Acids are often utilized

in agriculture for various purposes, such as soil pH adjustment, nutrient solubilization, and disease prevention. Typical acidification processes include sulfuric acid production, where sulfuric acid (H_2SO_4) is produced through inputting heat energy or burning sulfur containing minerals. Sulfur dioxide is the oxidized to produce sulfur trioxide (SO_3) which is then absorbed in concentrated sulfuric acid to form oleum and dileuted in water to produce the desired concentration of sulfuric acid [119-121].

The Ostwald process on the other hand is utilized to produce nitric acid (HNO_3) and is often used as an agriculture fertilizer component as well as other applications. Ammonia (NH_3) is oxidixed to nitrogen dioxide (NO_2) using either platinum or rhodium catalyst. Thereafter, the nitrogen dioxide reacts with water to produce nitric acid and nitrogen monoxide (NO) and then recycled back into the process [122-124].

These acids and others once produced are diluted to appropriate concentrations and applied to soil or crops. Thus, proper application techniques are necessary and important to ensure effective results without harming the environment or the health of those applying the acid. The common thread that connects these acidification processes is the various steps necessary to produce the acid and then deliver to the crops, which requires a significant amount of energy input in various forms. Thus, whether it is introducing ammonia in the form of solid fertilizer or control the

pH of soil while also introducing nutrients to the crops it is evident that energy plays a large role in the growth of crops and more alternatives are necessary to effectively grow crops for our increasing population. A more effective process is necessary to either contribute to growth of the plants either through introduction of nutrients or by also introducing acidity into the soil.

Chapter 2

Dielectric Barrier discharge atmospheric pressure nonequilibrium plasma jet combination configurations for irrigation water enrichment consideration

Nitrogenous fertilizers have contributed to the over nitrification of freshwater and ocean life, with the effects only seen in the past decade. The nitrogen in many compound fertilizers is in the form of ammonium (NH^+_4) form but depending on the temperature it can be changed by bacteria in the soil to nitrate. Plants such as cereals take and respond to the nitrate NO_3 anions quicker than the ammonium cations, while others respond as equally to either of the ions. The study of the in-house DBD plasma source was conducted, where different parameters of the discharge were analyzed for three different configurations for irrigation water enrichment consideration. The plasma mode observed varied as a function of input power, the presented work uses a constant input frequency of 26.5 kHz while varying physical parameters of the reactor such as ignition gap, flow rate, and volume treated. Characterization of the reactors is done using the power dissipated in the plasma, energy yield of nitrate ions, and nitrate injection rate. In addition, two of the reactors were utilized for a parametric study to determine if the plasma chemistry or behavior varied as a function of gap size and flow rate of Argon gas. Preliminary results are presented for the reactors below.

2.1 Introduction

With an ever-increasing global population, there is a constant emphasis on increasing our agricultural production and yield in order to be able to provide food to everyone. Agricultural production has increased several-fold during the last few decades with the help of nitrogen fertilizers developed using industrial processes such as Haber-Bosh. The Haber-Bosh process is the hydrogenation of non-reactive N_2 to produce biologically available ammonia (NH_3) which is a reactive nitrogen compound. As the population increases exponentially, it is estimated that agriculture production will have to increase approximately 70-100% to feed the population by 2050. Current agriculture systems that use such fertilizers are inefficient with their nitrogen use, losing 50-70% of applied reactive nitrogen to the environment [25-28] through several processes. One of the most important processes that contributes to this loss is eutrophication, the runoff from farm outflow, which is a product of the surplus water provided by either excess irrigation or rainfall that washes the excess nutrients to flow toward the world's estuaries [29]. The excess nutrients that not only include nitrogen, but also phosphorous and potassium that are swept away through such agriculture runoff. Additionally, eutrophication generates greenhouse gases and pollution through losses to the atmosphere and threatens

biodiversity and soil health [26,30]. Harmful algal blooms (HABs), for example, occur when simple photosynthetic organisms that live in estuaries grow out of control while producing toxic or harmful effects on people, fish, shellfish, marine mammals, and birds. The algae grow and take in higher concentrations of oxygen and create, what are referred to as, "dead zones" which are areas of water with less dissolved oxygen that ultimately causes fish to migrate and other organisms within the ecosystem to die [31-32]. Thus, it is imperative that alternative technologies for production of reactive nitrogen are introduced to meet the demands of future agriculture production.

Low-temperature plasma technology has been playing an increasingly active role in agriculture over the past two decades with several studies conducted in nitrate concentration increase, alkalinity reduction, plant growth enhancement, and pH regulation [33-38]. In addition, plasmas have been used as an enabling mechanism in medicine, food processing, plasma-based water purification, and microorganism removal in sea water [39-42] all of which represent the growing importance of plasma technology in biological applications. One of the primary reasons for the successful application of plasma technology in all these areas is the chemically active nature of low-temperature plasmas. This is largely enabled by the non-equilibrium nature of these plasmas with a significant mean energy difference between the heavy particles (ions and neutral species) and electrons. The energetic

electrons drive several desirable chemical reactions in plasmas ignited in air leading to the formation of reactive nitrogen and oxygen species which play a key role in several chemical processes that are of relevance to these biological applications. While the common feature of all low-temperature plasmas is the generation of reactive oxygen and nitrogen species (RONS), they can be ignited using a variety of approaches and configurations. For example, plasma reactors used for biological applications can be broadly classified into two major categories – atmospheric pressure plasma jets (APPJs) and dielectric barrier discharge (DBD) – with the choice of the reactor depending, to a large extent, on the specific objectives of the desired process. Specifically, several studies have shown that DBDs can generate abundant amounts of RONS from ambient air [43-46]. In contrast, certain studies have shown that APPJs are not as effective for delivering RONS for agricultural applications due to the small plasma plume that limits the active zone [47,48]. Overall, several studies have been conducted in which either of the two have been used to treat water, plant seeds, and even soil, resulting in increased growth rate of plants, disinfection of seeds, and seed coat modifications to increase water uptake [26,49-52]. A common theme in a number of these studies is the use of low-temperature plasma as an additional tool for the experimental group (with no plasma exposure for the control group) and correlate enhanced growth characteristics. Energy consumption that will remain an important bottleneck for the expansion of plasma-assisted agriculture to larger scales

and has only been considered by a few of these studies. In essence, the focus of a number of these publications has been to demonstrate increased growth due to the role of RONS delivered by the plasma to the plants with limited efforts to minimize energy consumption for the generation of these reactive species. In this regard, this study places emphasis not only on the generation and delivery of RONS but also on the power input to the plasma to produce a desired effect. The overarching goal of this study is to design and optimize nitrate injection in irrigation water using a hybrid DBD-APPJ set-up that combines the benefits of both plasma reactors and is feasible for large-scale treatment. Specifically, three different laboratory-scale plasma reactor configurations for water treatment are considered, with the overall goal of injecting nitrate ions through plasma treatment. The reactor configurations are characterized and assessed based on their power requirement per nitrate ion produced in the treated water. Parametric studies of various geometrical properties are also considered with the goal of making design choices in order to optimize the injection of nitrate ions into the treated water.

Experimental Set-up and Methods:

In this study, we focus on three different plasma reactor configurations for the treatment of irrigation water with each of the configurations described in detail below.

Various DBD-APPJ-jet configurations were considered and characterized based on plasma power absorption, nitrate injection rate into the treated water, and energy requirement per nitrate ion injected into the water. The primary independent variable that was used to characterize the performance of each reactor was the volume of water being treated. It should be noted that the volume of water also affects the thickness of the water layer which is an important geometric parameter for some of the configurations considered here. Once the reactors were characterized, we also performed other parametric studies to study the quantitative effects of other geometric parameters including carrier gas flow rate, and distance between electrodes. Each of the reactor configurations and the studies performed on them are described in more detail in the following paragraphs.

Reactor A: "Coaxial" DBD-jet configuration

Generally, a coaxial DBD consists of two flanges with an inner electrode and an outer electrode wrapped around a dielectric material. This reactor geometry allows for gas flow between coaxial cylindrical electrodes in such a way that allows for gas to be treated uniformly and thus generally used for large volume gas reactant treatments, such as reformation of methane or carbon dioxide [53-54]. The Coaxial DBD-jet reactor proposed in this study differs from the traditional Coaxial DBD configuration and uses a 250 mL beaker as the dielectric and a copper sheet wrapped around the beaker that acts as the powered electrode. For each study, it was ensured that the top of the copper sheet was at the same level as the surface of the water thereby ensuring that a single height parameter (distance between capillary tube exit and the surface of the water) could be used to describe the configuration. The beaker s then placed below a capillary tube which acts as the grounded electrode. The beaker is filled with the water that is to be treated and the entire set-up is under ambient conditions. The capillary tube electrode has argon gas flowing through it to assist with the plasma ignition thereby contributing to the jet characteristics of the set-up. Figure (5) shows a schematic of the DBD-Coaxial Jet that is referred to as reactor A in all the discussion presented here.

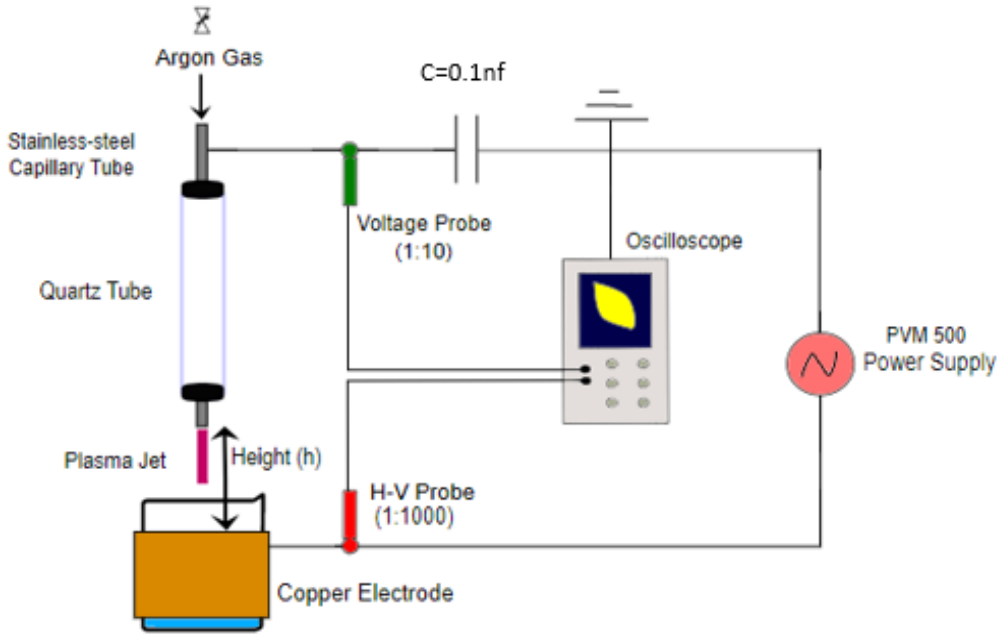

Figure 5.Reactor A Coaxial DBD-jet equivalent circuit.

Reactor B: "Pin-Plane" DBD-Jet configuration

Pin-plane type of reactors have been studied for water treatment in DC, AC, and other modes with results varying depending on the mode of ignition [55]. Unlike pin-liquid or pin to plate configurations reported in literature, the proposed DBD-jet reactor replaces the pin end of the electrode that is held within the quartz tube with a stainless-steel capillary tube. The powered electrode is located under the beaker with the capillary tube acting as the grounded electrode. As in the case of reactor A, argon was the carrier gas that flowed through the capillary tube and assisted with the plasma ignition. This set-up is referred to as reactor B in all discussion that is presented in this work. To reiterate, the primary difference between reactor A and reactor B is the location of the powered electrode. Specifically, the powered electrode in reactor A resembles a coaxial set-up, while the powered electrode in reactor B is planar. The distance between the powered and ground electrodes, in this case, will depend on the volume of water being treated. We believe that the primary advantage with both reactor A and reactor B configurations is the inherent role played by the treated water in the ignition of the plasma. This method of nitrate delivery can be expected to be more efficient than traditional jet-based configurations where the reactive oxygen and nitrogen species are delivered to the water as plasma effluents. A schematic of Reactor B shown in Figure (6) with the planar electrode exaggerated for visualization purposes.

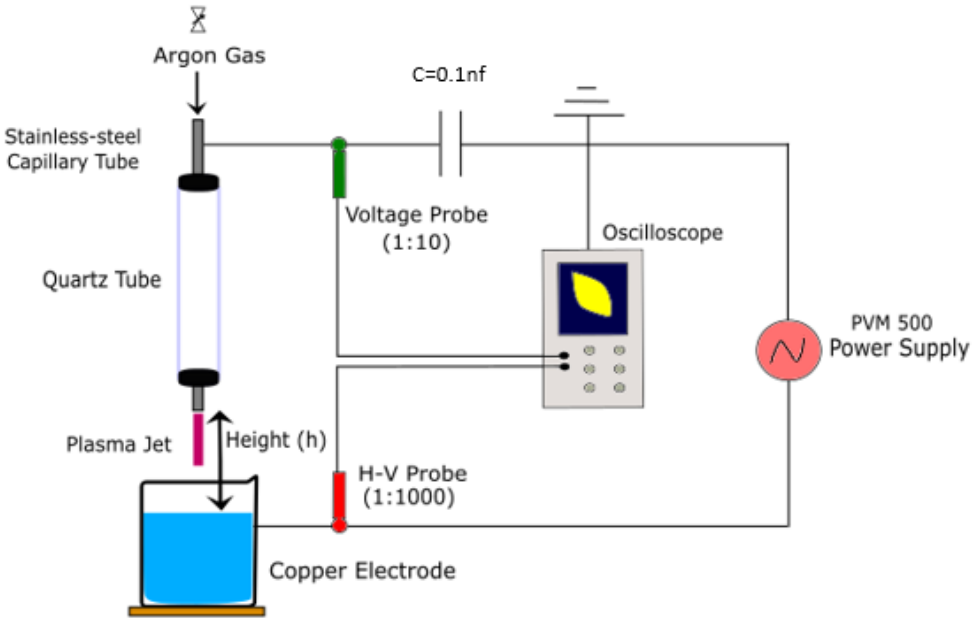

Figure 6. Reactor A pin to plane DBD-jet equivalent circuit.

Reactor C: "Pin-Plane" DBD configuration

The third reactor configuration that was considered in this work resembles a needle-plane set-up with a single needle like electrode in parallel to the plane electrode. Figure (7) shows a schematic of this configuration. Unlike Reactor A and B, the flow for Reactor C travels along the quartz tube. This would be qualitatively like traditional plasma jet configurations such as those used, for example, in several previous studies [59-61]. It should be noted that this configuration, follows the same height measurement from needle to surface of water.

Finally, it should be noted that this is not an exhaustive list of configurations possible but provides a good representative sub-set of DBD-jet hybrid configurations with similarities between the configurations but also sufficient variation from one set-up to another. To summarize the configurations, all reactors involve flow of argon gas through a capillary tube that acted as the grounded electrode. A second electrode either attached to the beaker (reactors A and B) or in proximity to the grounded capillary tube (reactor C) acts as the powered electrode.

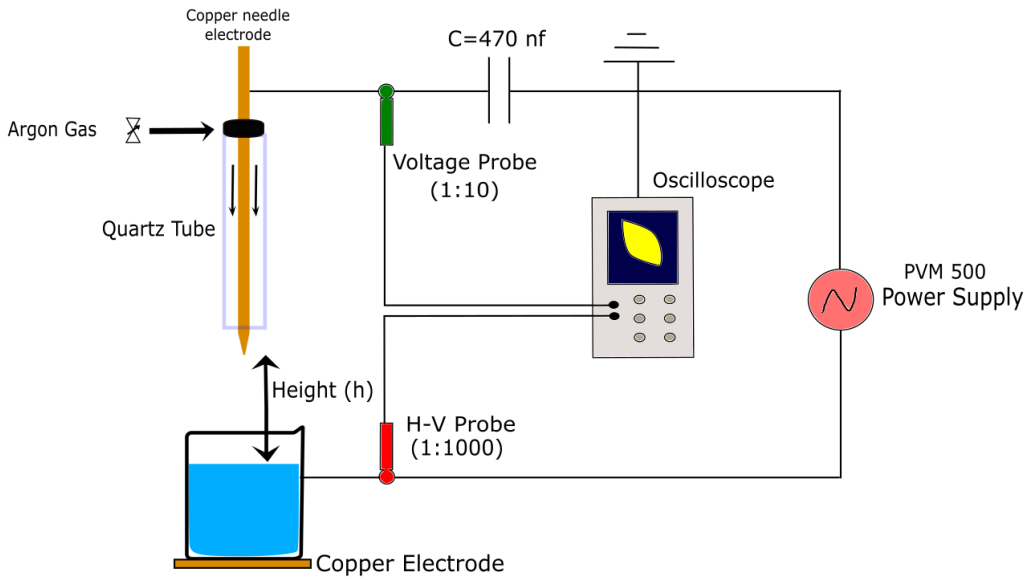

Figure 7.Reactor A pin to plane DBD equivalent circuit.

.

The power measurements were performed using the Lissajous approach [62-65] that allows for the current of the reactor, modeled as a capacitor, to be measured at a shunt high voltage (2kV) capacitor with 470 nF. The powered electrode and grounded electrode were both connected to a PVM 500 AC power supply (Information unlimited). The voltage of the reactor was measured using a high voltage probe (Cal Test Electronic, CT4028), while the charge of the shunt capacitor was measured using a passive voltage probe. Both probes were connected to a Siglent SDS1104xE digital oscilloscope utilized in x-y mode to obtain the Lissajous figure.

The nitrate concentration was measured using a Horiba LAQUAtwin compact nitrate ion meter with a $\pm$0.05 percent error. The grounded electrode was a capillary tube of 3.175mm inner diameter inserted inside a Quartz tube and two rubber stoppers that allowed the capillary tube to be centered. The capillary tube was connected to an elbow connection that was then connected to a John Smith flow meter that was then connected in series with an Argon tank of 99.99% concentration.

Results and Discussion

This work performs two different studies in order to characterize the reactor configurations described above as described in detail below. This section presents the results of both characterization and parametric studies of reactors A, B and C with an emphasis on power requirements for nitrate injection in the treated water.

Characterization of DBD-Jet plasma reactors

The initial study involved the characterization of the three DBD-jet reactors to determine nitrate injection rate dependence in the water layer thickness. To begin with, each reactor was studied for a constant capillary tube to water surface distance of 25 mm while varying the treated water volume from 50, to 125 mL in increments of 25 ml. The argon gas flow was

kept constant flow at 7 l/min. The plasma was ignited at an excitation frequency of 26.5 $\pm$ 0.5 kHz. Though the frequency remained constant for the study, the peak-peak voltage changes as a function of water volume. Deionized water was used for all the treatments with the nitrate concentration measured before and after plasma treatment to determine the rate of nitrate injection. The nitrate concentration was measured using a nitrate sensor as mentioned above.

To reiterate, the characterization of the reactors changed the water volume, which, for reactors A and B directly changed the distance between the electrodes. While the distance between the electrodes is independent of water volume for reactor C, there were still some changes in the distance between the electrodes due to constraints introduced by the beaker walls. However, this change in electrode distance is not very significant particularly when considering the change in distance between electrodes for reactors A and B. Figure 8 shows representative images of the three reactors when ignited at an excitation frequency of 26.5 kHz. It should be mentioned all three reactors operated in a streamer mode at these conditions even though it was possible to operate them in a jet mode at other conditions. The interaction between the plasma and the treated water was also captured using a Phantom V2512 high speed camera for as shown in Figure 9 demonstrating the typical streamer propagation characteristics from Reactor B in a time lapse at nanosecond scale. The V2512 camera is capable of

capturing 25,000 frames per second at a resolution of 1280x 800. The images taken are captured at an interval time of 1000 nano seconds and exposure tome of 900 nano seconds. The recording was approximately 12 seconds long and the height captured between the water and the stainless-steel tube was approximately 25 mm. Utilizing the parameters and from the camera and the operating distance of the reactor we can approximate the velocity of the streamer in the figure to be approximate $1.75x10^5$ m/s.

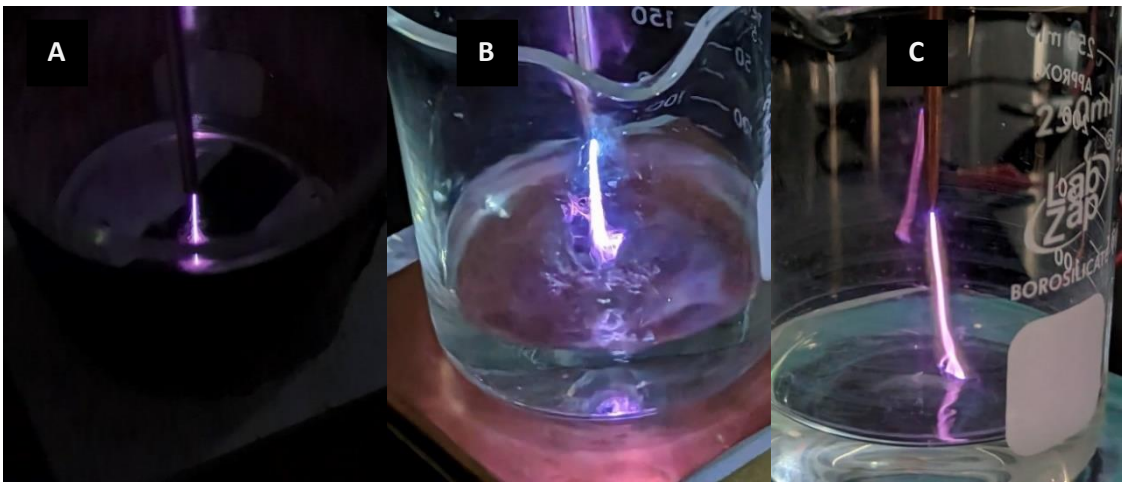

Figure 8.Plasma ignition of Reactor A, B, and C ignition at a constant frequency of 26.5 kHz and varying applied voltages.

Figure 9. Single streamer propagating from capillary tube electrode at an average velocity of 1.75 x 10^5 m/s.

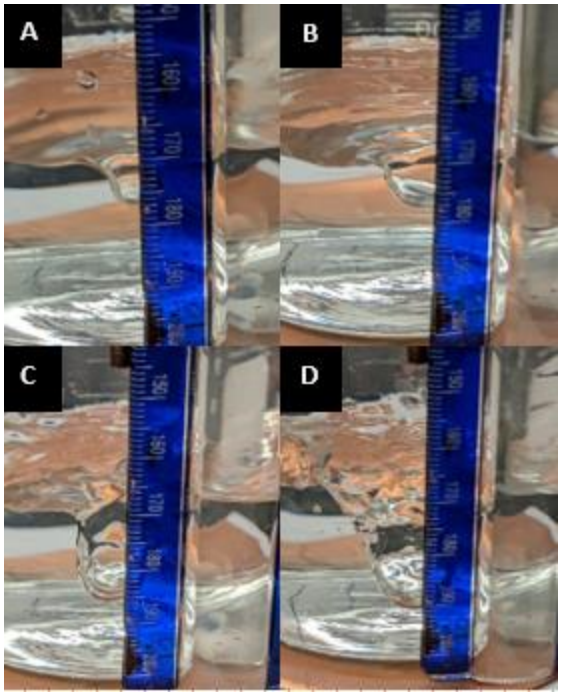

Figure 10.Argon fluid flow evolution; A) 3 slm, B) 5 slm, C) 7slm, D) 9slm for a volume of 50 mL filled 250 mL beaker which indicates a turbulent flow development for a constant height of 25 mm.

The characterization of the three DBD-APPJ configurations was performed on three parameters - power delivered to the plasma, nitrate injection rate, and energy yield defined as the mass of nitrate ions delivered per kJ of energy delivered to the plasma. While the plasma power was measured using the Lissajous method, the nitrate concentration in the treated water was measured using the nitrate sensor. The energy yield was computed based on the nitrate concentration and the power absorbed by the plasma and is given by

$$Energy\ Yield\ \left(\frac{mg}{kJ}\right) = \frac{m_{NO3}}{Pt} \quad (4)$$

where m is the mass of nitrate ions in the treated water, P is the power delivered to the plasma and t is the treatment time of water with plasma. It should be mentioned that all experiments were performed at nearly the threshold breakdown power in order to minimize power delivered to the plasma. While increasing power would increase nitrate injection to the treated water for all reactor configurations, the focus was on expending the minimum power to each reactor. Therefore, the operating power for each

reactor is also the breakdown power for the specific configuration. The experiments were conducted for water volumes of 50 mL,

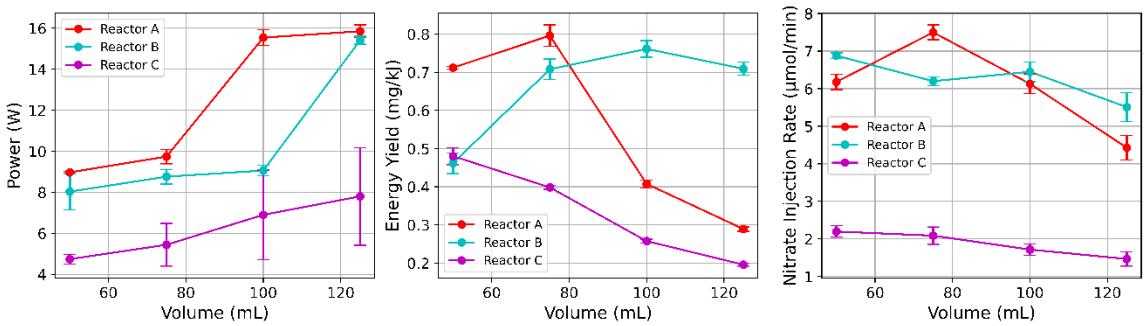

Figure 11. Reactor A, B, and C power, energy yield, and nitrate rate of injection comparison for a flow rate of 7 slm and a surface to electrode height of 25 mm

75 mL, 100 mL, and 125 mL and a constant argon flow rate of 7 slm. The capillary tube electrode was set at 25 mm from the water surface for all reactors. The nitrate injection rate into the water was calculated by obtaining the nitrate concentration with a nitrate sensor and it was measured periodically to obtain a change in time over the 600 second duration of water treatment. The results for the characterization of reactors A, B, and C are summarized in Figure (11).

The threshold power for plasma ignition increases for reactor A at about from approximately 9 W at 50 mL to 16 W at 120 mL of water. Similarly, reactor B resulted in a gradual increase in breakdown power which can be attributed to the increase of volume in the beaker. With increasing power input there is an increase in electron impact reactions in the plasma

that result in a higher number of excited states in the plasma, but increasing volume also decreases the concentration of ions present which results in the decrease of nitrate injection for all reactors. Specifically, the electrode being located under the beaker results in an increase in electrode separation by about 4 mm as the water volume increases from 50 ml to 125 ml. Lastly, reactor C also demonstrated an increase in power delivered at breakdown which can be attributed to changes in the electrode to plane separation resulting in an increase of power from approximately 5 W to 8 W. The needle to plane DBD configuration develops into a corona discharge where the charge particles are accelerated toward the plane electrode. The power dissipation for this configuration can be relatively low compared to the other reactors. Since the plasma discharge occurs primarily at the needle tip, the plasma volume is limited, resulting in lower power consumption. However, the power dissipation still depends on the applied voltage, gas pressure, and other operating parameters, in this study the focus remained on consuming the least amount of power. This can be accomplished by adjusting the power supply to supply enough voltage to breakdown the plasma, in each case presented the minimum applied voltage was applied for plasma ignition, resulting in lower ionization due to the smaller volume of plasma compared to reactor A and B.

The rate at which nitrate ions are introduced into the reactor was computed based on nitrate concentration measurement, the volume of water treated and the treatment time and is given by

$$r_{NO_3^-} = \frac{[NO_3^-]}{Vt} \quad (5)$$

where $[NO_3^-]$ is the concentration of nitrate ions, V is the volume of the treated water and t is the treatment time. Reactor B has a nearly constant injection rate which is consistent with the fact that the water dielectric thickness plays a negligible role in determining the electric field distribution in the gap between the capillary tube and the water surface. Therefore, for this configuration, the electron-impact reactions are least impacted by the volume/thickness of water in the beaker. The small variations in the injection rate can be attributed to small variations in the power delivered to the plasma. With nitrate ion injection rate being constant, the energy yield is independent of the volume of water and is estimated to be about 0.75 mg of nitrate ions per unit energy delivered to the plasma. On the other hand, the nitrate ion injection rate demonstrates a decrease with increasing volume of water for reactor A where the electrode separation and the water dielectric layer thickness increase with increasing volume of treated water. As a result, despite the increase in power delivered to the plasma (as a result of the increase in breakdown power), the gas-phase reactions are less efficient in producing the nitrate ions. With the nitrate ion injection rate can be lower

due to inefficient transport of nitrate ions to the surface of the water, we do not attribute the lower injection rate of reactor B to reasons involving transport since the gas flow and hence species transport is nearly identical between reactor A and B. Therefore, we attribute the lower injection rate of nitrate ions to lower production of nitrate ions in the gas-phase which in turn is potentially due to lower mean energy available to electrons to drive these gas-phase reactions. The lower production of nitrate ions in the gas-phase becomes increasingly significant as the volume of water increases and with the accompanying increase in power delivered for sustenance of the plasma, the energy yield drops drastically as the volume of treated water increases. Reactor C on the other hand, has a decreasing rate of nitrate injection with increasing volume and an increasing power consumption, thus increasing the energy yield from approximately 0.5 mg/kJ to 0.2 mg/kJ.

Influence of Electrode to Water Surface Height

In addition to characterizing the reactors in terms of nitrate injection rate into the treated water, reactors A and B were further studied to determine the influence of geometric and flow parameters. DBD ignition is strongly dependent on the applied electric field which in turn depends on the distance between the two electrodes. Therefore, we first performed a parametric study by varying the distance between the capillary tube and the

water surface. Specifically, the distance was varied from 15 mm to 30 mm.. The other parameter that was varied as part of this study was the argon flow rate through the capillary tube. As discussed earlier, argon was used as a carrier gas to assist with the plasma ignition. The flow rate of argon would therefore play an important role in the plasma dynamics. While detailed diagnostics are beyond the scope of this work, our emphasis is on the role of argon flow rate on the delivery of nitrate ions to the treated water.

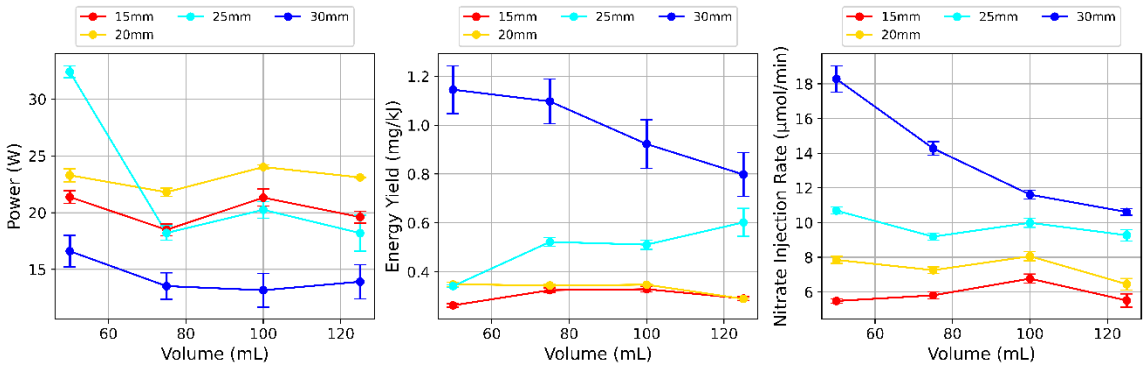

Figure 12.Reactor A power, energy yield, and nitrate rate of injection comparison for various heights at a constant flow of 7 slm.

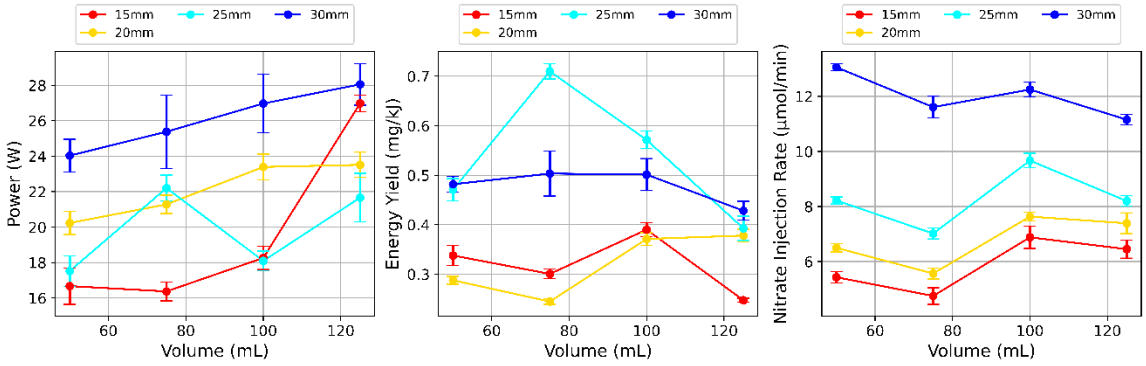

Figure 13. Reactor B power, energy yield, and nitrate rate of injection comparison for various heights at a constant flow of 7 slm.

The resulting power dissipation, energy yield and nitrate ion injection rate are reported in Figure (12) and Figure (13) respectively. With respect to power dissipation, Reactor A, whose geometry mimicked that of a coaxial DBD in which the stainless-steel tube acted as the inner electrode and the outer electrode was wrapped around the beaker. The distance was varied for the surface of the water from heights ranging from 15 mm to 30 mm.

The increase in height results in an increased electric field necessary for breakdown and thus with increasing power dissipation there is an increase in power consumption for all reactors. While most heights showed a slight variation of power of about 2 W, the 25 mm height for reactor A had a power dissipation of about 33 W for a volume of 50 mL, with a decrease of approximately 12 W for 75 mL and varying slightly for 100 mL and 125 mL. The surface to electrode height of 30 mm for reactor A, had the higher energy yield for every nitrate ion inject of approximately 1.1 mg/kJ, indicated a high degree of oxidation of both oxygen and nitrogen which would in turn produce species such as nitrate with an increase in energy input. Reactor B on the other hand, had a power dissipation higher for 30 mm height between the electrode and surface of the water. The power increases as a function of volume, but variance is introduced as a function of height, which may be due to the influence of the argon flow, whose turbulent nature increases with decreasing height affecting the plasma ignition and thus power dissipation. Furthermore, the distance of 30 mm also yields the highest rate of injection of

nitrate ions, but the power increase with volume results in an energy yield lower than equal to or less than 15 mm and 20 mm and varying slightly with a height of 25 mm. The turbulent flow gives rise to an oscillating electric field which causes plasma to become transient when the flow of 7 slm lowered to heights of 15 mm and 20 mm. For the case of Reactor B, the electric field varied vertically between the plane electrode and the capillary tube electrode, while Reactor A had an electric field that varied on the distance between the electrode wrapped around the beaker which remained constant, aside from slight deviations caused by oscillations from the flow passing through the tube and varied based on the distance of capillary tube placed inside of the beaker. This is explored in the next section of the manuscript to understand the oscillatory nature of the flow on the water and the transient mode of the plasma observed due to this motion.

Influence of flow rate

Further exploration of the flow was conducted to further understand the effect of the argon flow on power dissipation, energy yield and nitrate ion injection for both reactor A and B. Observation of Figure 11 which shows the flow evolution of argon on the water surface in a volume of 50 mL indicates that the induced flow is close to laminar for flow rates of 3 slm and 5 slm, with a height of 25 mm being held constant and in between a transition

exists that causes the argon bubble developed in the water to deviate violently with increased flow rate. The study then further analyzed the plasma characteristics as a function of this flow phenomena observed.

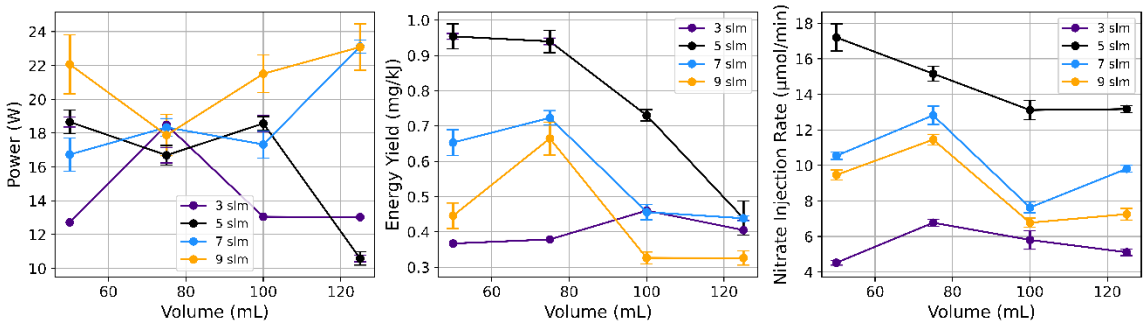

Figure 14. Reactor A power dissipation, energy yield, and nitrate rate of injection comparison for operating flow rates of 3, 5, 7, and 9 slm at a constant height of 25mm

Figure (14) summarizes the results for the coaxial DBD like reactor or Reactor A. The power dissipation seemed to be higher for flow rate of 9 slm with a dissipation of approximately 22.4 W for a volume of 120 mL. The introduction of more gas molecules increases the number of particles per unit volume between the capillary tube electrode and the surface of the water.

Furthermore, there electric field distribution can also be affected by an increase of argon flow due to the increased velocity or flow rate, where higher gas velocities can alter the gas dynamics and modify the electric field near the dielectric surface. In the case of reactor A, the dielectric beaker encapsulates the flow of argon and surrounding air causing an erratic electric

field causing the power oscillations observed in Figure (14). Furthermore, plasma ignition observed at a flow rate of 9 slm was observed to be erratic with a nonuniform streamer propagation. As the argon flow rate decreased the ignition was observed to uniform within the argon bubble.

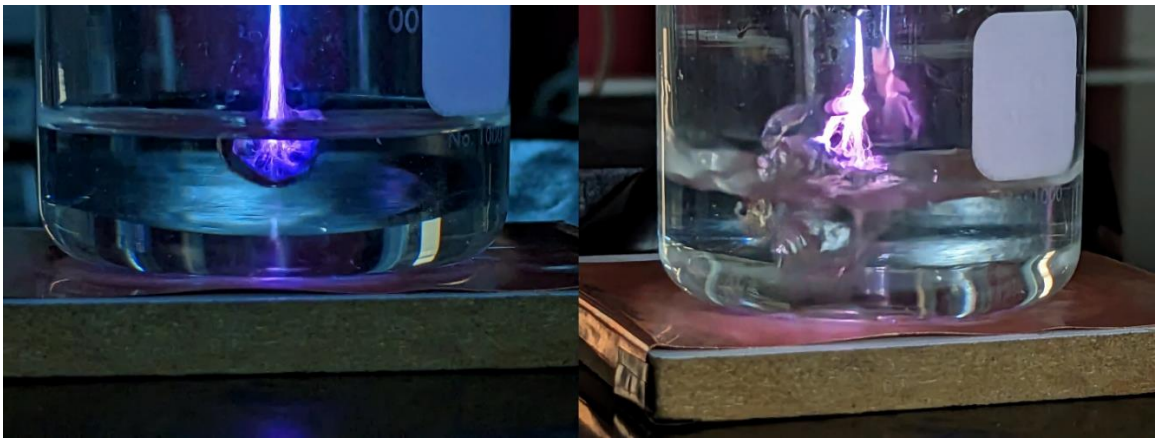

Figure 15.Reactor B plasma ignition for a volume of 50 mL, frequency of 26.5 kHz, (left) flow rate of 5 slm, (right) flow rate of 9slm.

Figure (15) consists of Reactor B plasma ignition at flow rates of 5 slm and 9 slm. At a flow rate of 5slm it can be observed that the argon flow developed creates a small hemispherical bubble within the water in both Figure 6 and Figure (15). The ignition is almost uniform within the bubble and microdischarges from the streamer propagation of the nonequilibrium jet can be observed inside of the bubble. The same behavior was observed for reactor A, but due the outer electrode covering the outer transparent walls of the beaker, it made taking an image of the cross section difficult, but a similar behavior was observed for Reactor A.

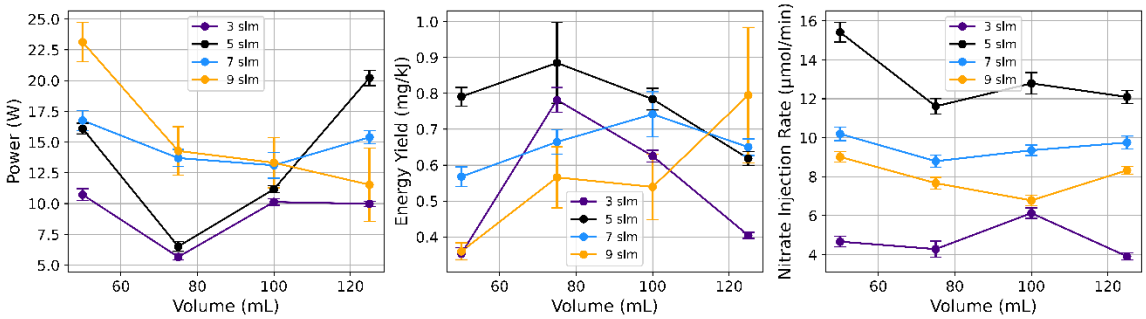

Figure 16. Reactor B power dissipation, energy yield, and nitrate rate of injection comparison for operating flow rates of 3, 5, 7, and 9 slm at a constant height of 25mm.

Reactor B also dissipated an increased amount of power with increasing flow rate of argon gas with a power of approximately 23 W for 50 mL and a nitrate injection rate of approximately 9 µmol/min resulting in a low energy yield per ion injected as shown in Figure 16. The variability developed for higher flow rate may arise from captured data time as the inconsistency of ignition rose with increasing flow rate. In both Reactor A and Reactor B a flow rate of 5slm seems to have the higher efficiency of converting the electrical energy into production of ions. This flow rate seems to increase the amount of reactive oxygen and nitrogen species in the plasma increasing the rate of injection while maintaining a relatively low power dissipation due to the uniformity of the plasma ignition caused by the flow of the argon in the water.

Conclusion:

DBD-jet configurations with an inner stainless steel capillary tube electrode and gas delivery system were characterized for irrigation water consideration via power dissipation, nitrate rate of injection, and efficiency of nitrate delivery.

The power dissipated increases as a function of water height or volume in the beaker while keeping parameters such as flow rate, height, and frequency constant. Additionally, Reactor B injects the most nitrate ions while maintaining a relatively low power dissipation. The argon flow certainly affected the ignition process of the plasma as it consists of lower breakdown voltage making the plasma ignition efficient even at ambient conditions. The combined effect of the jet plasma plume and the dielectric barrier discharge were introduced at frequency of 26.5 kHz for all reactors. DBD-jets introduced in this study can be used to treat water at various volumes and scaled up for agricultural usage while maintaining a relatively low cost of use for communities that lack funding for complex irrigation systems.

Chapter 3

Application of a dielectric barrier discharge atmospheric pressure jet for growth rate enhancement of vegetables

As of November 2022, the United Nations Department of Economic and Social Affairs, Population Division reported the total earth population had reached 8 billion. This growth is due in part by the gradual increase of human lifespan owing to improvements in public health, nutrition, personal hygiene, and medicine. Unfortunately, countries with the highest fertility levels tend to be those with lowest income per capita [67] and with increased fertility a need for higher food production follows. Additionally, the rise of hunger in the world increased by over 150 million people from 2020 to 2021 according to the Food and Agriculture Organization of the United Nations with a prevalence of undernourishment being greatest in African countries [68]. Increasing food production is a necessity in the world, but with increasing food production comes with both positive and negative effects on the environment and health. To begin with, in terms of the environment there are several factors to consider for agriculture which include the potential abuse of chemical fertilizers and pesticides, which are capable of not only affecting the agricultural ecosystem but also may affect the growth and development of crops [69-71]. Furthermore, pesticides may also pose a health risk to agricultural workers who handle and apply them, as well as the

consumers who are exposed to pesticides residues on food. These include pyrethroids such as bifenthrin and permethrin, which are synthetic pesticides to control a wide range of insects that may also include indirect targeted insects. Human exposure to such pesticides has been linked to skin an eye irritation, respiratory issues, and potential effects on the endocrine system [72-73]. In addition, chemical fertilizer abuse can also contribute to potential nutrient imbalance and soil degradation which affect the crop development. If certain essential nutrients are over-supplied while others are neglected, it can hinder the plant's ability to take up nutrients properly, affecting the growth and development [74]. Similarly, a frequent and excessive utilization of chemical fertilizers can degrade soil health over time through potential soil acidification, reduced organic matter content, and a decreased soil biodiversity, making the soil less fertile and less capable of supporting healthy crop growth [75-76]. Currently, governments impose specific set Maximum Residue Limits (MRLs) for pesticides, but with an increased number of people on the planet, policing such limits will become problematic for countries of low-income households. Similarly, chemical fertilization can be mitigated with sustainable agricultural practices that may include adopting balanced fertilization approaches, soil testing to determine nutrient needs, and employing integrated nutrient management strategies to ensure optimal crop development while preserving soil health and environment sustainability, but like pesticides these current practices

may require monetary resources and countries with the highest fertility do not have these resources to maintain the practices. Thus, the problem of limited resources and increasing populations requires an alternative solution that is relatively inexpensive to assist with the current food production methods in low capita countries.

To further assist in solving this problem, researchers must explore new avenues of study. In the past decade one of the most sought out types of technology that may serve as an alternative solution to food production is the application of non-thermal plasma technology in agriculture. Plasma is the fourth state of matter, whose make up can be defined to be high-energy particles that include electrons, ions, excited atoms, excited molecules, and free radicals. It has high oxidative properties can assist with the reduction of organic matter. Though plasma has been around for several decades now, its application in agriculture has recently come into light as an alternative to current practices held in agriculture. Low-temperature atmospheric plasma has been utilized for seed germination, plant growth, sterilization insecticides, virus inhibition, agricultural product preservation, and pesticide residue degradation because of its fat, efficient and pollution-free characteristics [77-81] reviews in detail the current role of nonthermal plasma in the development of plants from seeds to crops, which include a discussion the key developmental stages of plants and their needs. Plasma generators or reactors are developed to either be discharged at the surface of

a liquid such as water, in other instances the plasma is ignited in the liquid itself utilizing a strong potential electric field, and in both instances the presence of a gas flow such as an inert gas as argon can be introduced to reduce electric field potential necessary to ignite the plasma [82-84].

Plasma discharge in either instance mentioned above may produce a plethora of species depending on type of reactor and its specific configuration with respect to power delivery and gas type. For example, in an air discharge alone one may encounter various species are generated in the gas, such as nitric oxide (NO), hydroxyl radical (OH), superoxide anion radical (O_2^-), atomic oxygen (O), nitrogen ions (N_2^+), and excited nitrogen molecules (N_2^*). If the discharge encounters a fluid surface, for example water, other species are generated, and new products are formed at the liquid-air interface of the discharge such as hydrogen peroxide (H_2O_2), nitrate (NO_3^-), nitrite (NO_2^-), and ozone (O_3) [85]. The resulting volume of water that interacted with plasma is known as plasma activated water (PAW) [86-87]. The reactors utilized for plasma ignition range from plasma jets and plasma actuators that are driven by different sources of power and thus produce varying species from those mentioned above. Plasma atmospheric pressure jet and dielectric barrier discharge configuration type of reactors are two of the most common reactors in plasma agriculture [88-90].

This study aims at developing a further understanding to low temperature nonequilibrium atmospheric plasmas, more specifically we introduce an in-house design DBD configured atmospheric pressure jet (DBD-APPJ) that utilized an argon flow to ease ignition requirements, i.e., electric field, to produce PAW for various vegetable plants including *Raphanus sativus* (radish), *Capsicum frutescens* (hot pepper), *capsicum annuum* (sweet pepper), and *solanum lycopersicum* (tomato). The study aims at characterizing the PAW produced by this hybrid system, by reporting the properties of the water as a function of treatment time of plasma. These properties include, pH, nitrate ions, total dissolved solids (TDS), electrical conductivity (EC), and salinity. Furthermore, the study aims at reporting the electrical characteristics of the plasma as well as chemical information, which is reported via optical emission spectra. The spectra are utilized to obtain specific energy transitions such as N_2 ($C^3\Pi_u \rightarrow B^3\Pi_g$) as well as radical species produced during plasma ignition. This information is then utilized to calculate the rotational temperature and vibrational temperature of nitrogen and nitrogen ion bands through simulated Boltzmann plots. Lastly, regarding food production, the rate of growth in the vegetable plants is calculated for stem length, stem diameter, and number of leaves as a function time being grown of approximately 60 days providing an insight on increased rate of food production through utilization of PAW from the atmospheric pressure jet DBD.

Methodology:

Vegetable Plants and PAW conditions

The study of an atmospheric pressure plasma jet with a DBD configuration is considered for agriculture alternative to fertilizer and efficient growth rate enhancer for 4 different plants. As opposed to previous studies that utilize deionized (DI) water [91-93] this study provides data from tap water originating from the Sustainability Research and Engineering building at the University of California Merced. Unlike DI water, tap water may contain several substances such as chlorine, copper, and other potential reactive species according to the City of Merced Consumer Confidence Report 2022 which lists all potential substances found in tap water [94]. The PAW was produced by treating approximately 100 mL of tap water for a time of 5, 10, 15, and 20 min for multiple runs each to produce enough water for all plants in the 60-day time period. The seeds were obtained from Burpee Holding Company Inc. (Warminster Township, PA) and separated into 4 different pots filled with coco-coir (Dutchman brand, USA) which unlike soil does not provide additional supplementation, which would allow us to study the full effect of the PAW and the effect of the plants knowing that the supplementation is provided only through the water the plant absorbs. The pots are kept at approximately 12 inches from the grow lights and kept on for approximately 16 hours and turned off by use of a timed electrical outlet.

Germination rate can by dividing number of seeds that reach the seedling stage, which marks the early development phase of the plant's life, after it has successfully sprouted from the seed and established its root by the total number of seeds the study used. Germination can be observed prior to planting in the pot by watering the seeds 7 days in cotton sleeves as it is a simple and effective way to observe whether the seeds are able to transfer to the soil. Since the study utilized a sample size of N=6 for calculating averages, results presented may not provide proper statistical significance, but can be interpreted as random samples to show effect of PAW and the potential of the DBD-APPJ discussed thus far. Growth rate of the plants was determined by measuring the stem length once the plants surfaced from the substrate over an interval of 15 days until 60 days were reached. Furthermore, the study reports the numbers per the same interval for the 60 days. Germination, growth rate and frequency of leaf growth are influenced by the amount of nitrate absorbed during the plants growth cycles, thus an increase in either of these indicate the potential of nitrate ion injection of the presented DBD-APPJ.

DBD-APPJ electrical characterization

The in-house DBD-APPJ consists of a 3.175 mm outer diameter stainless steel capillary tube that acts as both the flow path of the argon and as one of the electrodes of the reactor. Following the capillary tube is a 250 mL borosilicate beaker and below a planar copper electrode where alternating current (AC) power is introduced to the system. The capillary tube is the connected to a flow meter adjustable between 0-20 slm with an accuracy of $\pm$ 0.10. The equivalent circuit diagram and DBD-APPJ configuration is shown in Figure (17)with proper measuring tools for analysis.

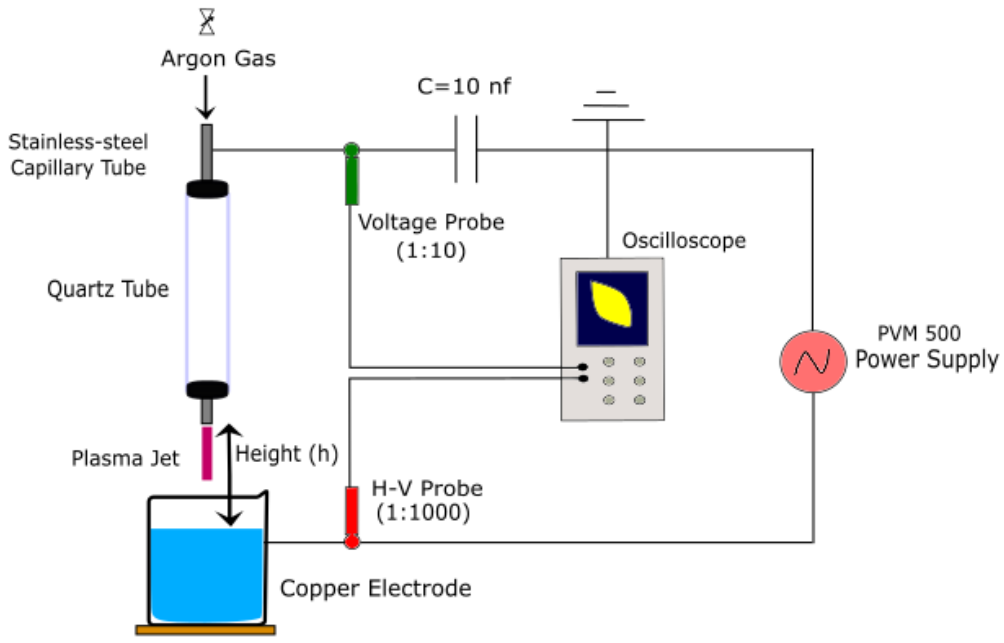

Figure 17.DBD-APPJ configuration and equivalent circuit diagram.

The AC power supply was ignited at a frequency of approximately 30 kHz and a height, which is the distance from the surface of the water to the edge of the capillary tube of approximately 25 mm. A constant flow rate of approximately 7 slm was chosen for the argon flow passing through the capillary tube. While the reactor ignited at various frequencies, flow rates, and heights the uniformity of the ignition based on our previous study. Electrical power was captured utilizing Lissajous method and waveform methods for this experiment to obtain average power dissipated from the plasma through utilization of;

$$P = \frac{1}{T}\int UIdt \quad (1)$$

$$P = \frac{1}{T}\int UIdt = \frac{C}{T}\int U\frac{dU}{dt}dt = fC\oint UdU \quad = FCS \quad (2)$$

Equation (1) utilizes the measured current and voltage to obtain an average power over a cycle, while equation (2) utilizes the charge from a capacitor C placed in series with the DBD-APPJ and the Lissajous figure is integrated over the area of the Q-V curve generated on the oscilloscope. U is the applied voltage and I is the current measured. The voltage is measured utilizing a high voltage probe while the current is measured with a Rogowski like current probe. The rate of change of charge of the capacitor in series is measured with a simple voltage probe and charge can be obtain by simply multiplying the voltage measured and the capacitance. Both methods were

employed as the DBD-APPJ plasma jet was not a "bullet" nor was it a series of streamers propagated like that in a typical DBD [95-96], thus employing both methods would provide us with a better insight to describe the combined effect of the reactor.

DBD-APPJ Plasma Chemistry Characterization

The DBD-APPJ plasma chemical characteristics were analyzed utilizing Optical Emission Spectroscopy (OES) (HR400 pro High Resolution Spectrometer, Ocean Insight) An optical fiber was fixed and focused at the DBD-APPJ to capture the electromagnetic radiation emitted from the plasma at wavelengths between UV-VIS (220-1100nm). OES has been historically applied to observe plasma to characterize the chemical species within it, additionally it also provides information about plasma energy distributions and kinetics. Past studies with APPJs have shown an increase in plasma temperature and electron density with input power or a decrease in plasma temperature with increasing distance [97-100]. An open source code (MassiveOES) was utilized to calculate the vibrational and rotational temperature [101-103] by

$$f_B(T_{rot}, T_{vib}, J', v', \alpha') = \frac{(2J'+1)\exp\left(\frac{E_v}{k_B T_{vib}} - \frac{E_J}{k_B T_{rot}}\right)}{Q(T_{rot}, T_{vib})} \quad (6)$$

$$Q(T_{rot}, T_{vib}) = \sum_{J', v', \alpha'} (2J'+1) \exp\left(-\frac{E_v}{k_B T_{vib}} - \frac{E_J}{k_B T_{rot}}\right) \quad (7)$$

Where J' is the quantum number describing the total molecular angular momentum apart from the electronic spin or the rotational quantum number, v' is the vibrational quantum number, α' is the fine structure component that needs to be distinguished for multiplets, f_B is the Boltzmann fraction, and k_B is the Boltzmann constant. The Boltzmann fraction is divided by Q to ensure that the fraction sum is equal to 1. E_v is the potential energy of the upper vibrational state that may also include the electronic state energy and E_J is the total energy of the upper state without the vibrational and electronic component or the energy of molecular rotation and all fine structure splitting effects.

Results/Discussion:

DBD-APPJ plasma electrical characterization

The discharge plasma observed between the surface of the water and the stainless-steel capillary tube consisted of a multitude of filaments or streamers that randomly were distributed within the argon bubble of the beaker. The resulting waveform is presented in Figure 18 along with the Lissajous curve pertaining to the discharge of the DBD-APPJ.

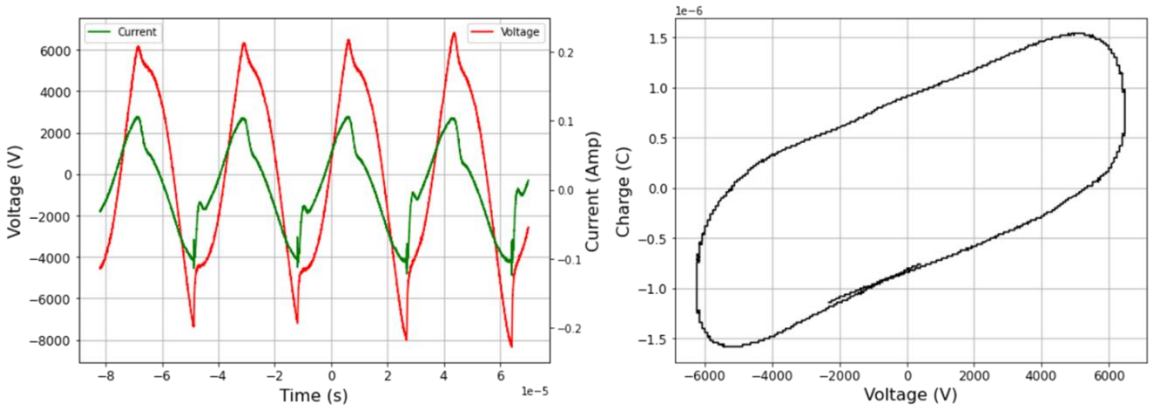

Figure 18.left) Current and voltage waveform (right) Lissajous figure for DBD-APPJ with a frequency of 30 kHz.

The voltage and current waveform method show a DBD like behavior with sharp current spikes that are representative of continuous streamers propagating from the stainless-steel tube. Furthermore, the Lissajous figure observed is like that of a typical DBD indicating that the relationship between a capacitor and DBD-APPJ holds true even when the flow of Argon is flowing from the capillary tube as opposed to the quartz tube as typical APPJs [104-106]. Utilization of Argon on the DBD with a height of 30 mm resulted in a peak-voltage of approximately 6.2 kV, which is expected since the argon breakdown is much lower than that of air. In addition, when considering the electric field produced between both electrodes, one must consider the geometry, while the bottom electrode is a plane, the top electrode is the circular surface from the capillary tube, that can be described as a thin ring which also contributes to the low potential. Furthermore, DBD plasma at smaller gaps typically results in higher power density and a more intense plasma discharge due to the concentration of electric field in a smaller

volume, but the in-house DBD-APPJ resulted in a more intense plasma under conditions where the gap was higher than 15 mm. This may be caused by the turbulent nature of the water when the flow of argon interacts. Overall, the power dissipation was calculated to be approximately 16 W by the waveform method and approximately 17.1 W for the Lissajous Figure, with a relatively low error with both methods, it is evident that either method can be employed to characterize the reactor.

DBD-APPJ plasma Chemical characterization

The chemical species of the plasma were studied by utilizing optical emission spectroscopy and the massiveOES code, that utilizes fits and quantum relations to estimate the rotational and vibrational temperature of the excited species of nitrogen diatomic molecules in excited state present in the plasma. Furthermore, the code was also able to provide energy transition information about the energy transition of the same molecule, specifically N_2 ($C^3\Pi_u \rightarrow B^3\Pi_g$) was observed in the spectra showed in Figure 19, in addition the vibrational temperature and the rotational temperature utilizing the upper energy levels are presented in the same plot.

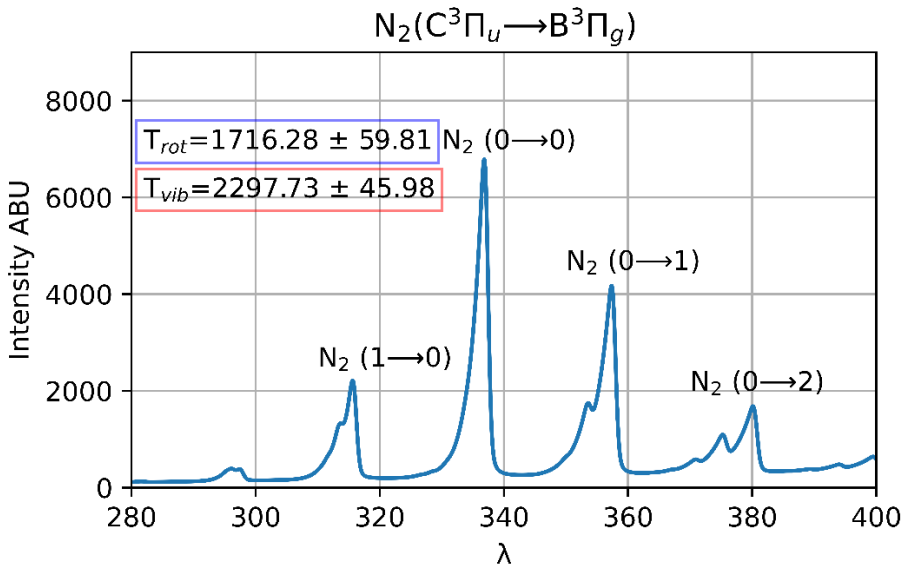

Figure 19. Optical Emission Spectroscopy emission spectra of DBD-APPJ for N_2 C-B energy transition.

By assuming a Boltzmann distribution, the code can fit the data to estimate the rotational and vibration temperature of the N_2 state observed with OES. The transition from the first negative system C to the second positive system B of molecular molecule N_2 is responsible for producing significant amount of excited N_2 molecules. This is relevant to understand the reaction pathway taken by the oxidized nitrogen and determine the role of activated nitrogen species, which vary in lifetimes, stability, and performance, can lead to an increase in ammonia production and highly efficient ammonia synthesis direction from the nitrogen gas and water [107]. Furthermore, the excitation of nitrogen molecules in the C-B transition can lead to the production of ozone (O_3) through reactions with oxygen molecules. Ozone is crucial in various application which includes air purification, water treatment, and its potential for preserving fresh vegetables [108]. While not

investigated, an ozone detector was utilized to test this theory and it was observed that during ignition the atmospheric concentration of ozone generation remained constant during plasma ignition, indicating that indeed there is ozone generation which perhaps is due to this vital N_2 transition.

Plasma Activate Water Characterization

The DBD-APPJ was operated at a constant set of parameters that included a height approximately 30 mm from the surface of the water and a frequency applied of 30 kHz. The study consisted of preparing PAW under these conditions for the plants for the duration of 60 days. A 250 mL beaker was filled with 100 mL of tap water and treated for times ranging from 5-30 min. The ionization potential of the plasma can be observed in both pH and NO_3^- production in Figure 20.

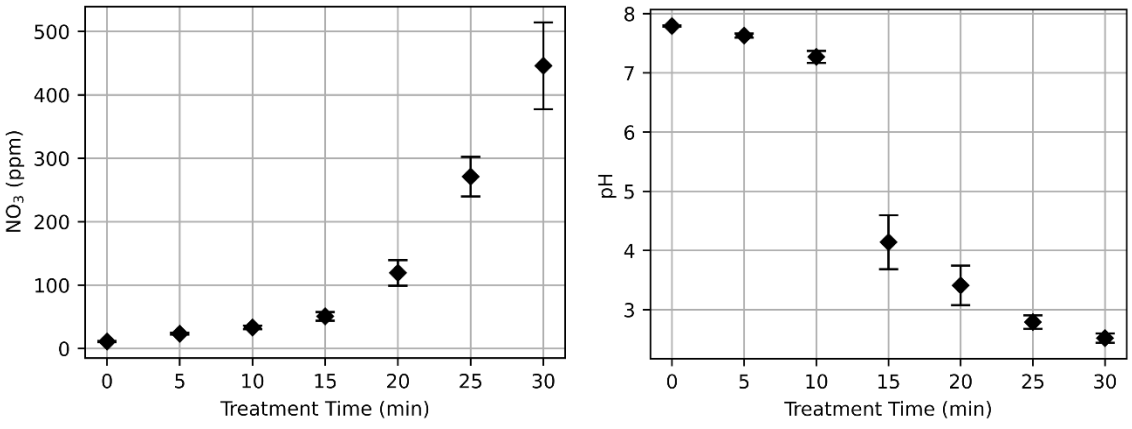

Figure 20.PAW pH and nitrate results indicating a high rate of ionization of water and air.

The results indicate that there is a high presence of H^+ ions for treatment time above 15 min, which may be a result of the plasma ignition stability which remained uniform for the entirety of the water preparation. The oxidative properties of plasma allow for plasma species such as hydroxyl radical (OH) and ozone (O_3) which both have strong oxidation potential. These species may encounter nitrogen containing compounds in the water and oxidize the nitrogen atoms converting them into nitrate ions. One example of this is ammonia (NH_3) which can be oxidize to nitrate (NO_3) through a series of reactions involving (OH) radicals. This may be the case for the DBD-APPJ under investigation as there is a seemingly exponential increase of NO_3^- ions in the water as treatment time is increased. While one cannot show the path the ionization will take under ambient conditions, it is possible to deduce and increase ionization potential by the plasma by simply analyzing the water properties before and after treatment, for electrical conductivity for example, shown in Figure (21). There is an almost 10-fold increase between tap water and PAW.

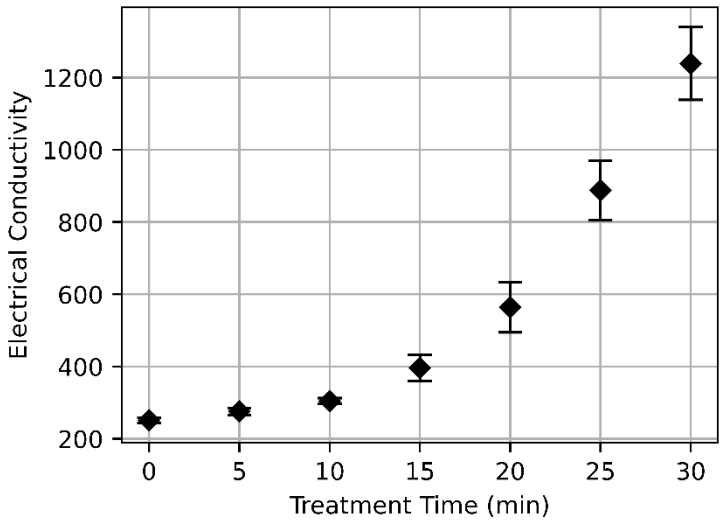

Figure 21.Electrical Conductivity of DBD-APPJ for plant growth enhancement.

The trend of increasing conductivity further indicates the presence of dissolved ions or an increase in the concentration of ionic species in the treated water. While an increase in electrical conductivity after plasma treatment does not necessarily indicate ineffective treatment, in many cases, the rise in conductivity might be associated with the removal or degradation of the organic contaminants and the transformation of complex molecules into simpler, more conductive ions produced by the plasma. While the latter may be true, increasing of electrical conductivity may also increase the salinity or concentration of ions such as sodium (Na^{+}), chloride (Cl^{-}), magnesium (Mg^{+2}), and sulfates (SO_4^{-}) among others. The level of initial salinity may or may not include any of these ions and can be affected by natural factors, such as geological formations and weathering processes, but for this study we focus on the value of no treatment and the PAW for various

treatment times. Figure (22) shows an increase in salinity as a function of treatment time.

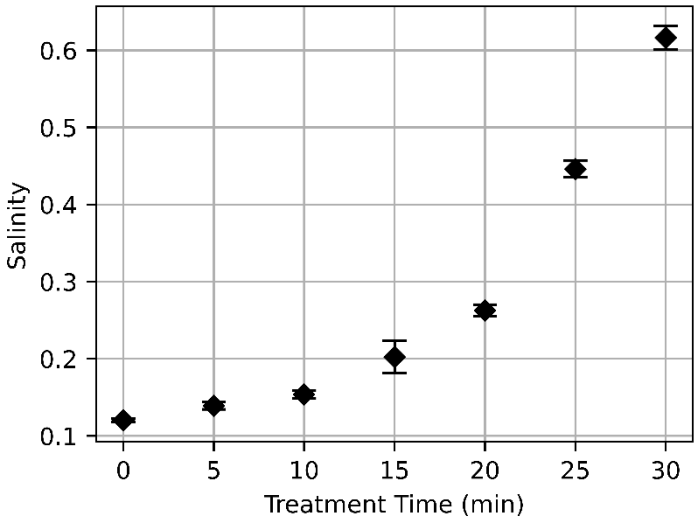

Figure 22.Salinity of tap water and various treatment times of PAW.

The reason for the increase of the salinity demonstrates the ionization of not only the air and water molecules, but also alkaline elements that are in tap water. An increase in electrical conductivity which correlates with an increase of charge particles from the plasma is a major contributing factor to this increase in salinity. Further investigation is necessary to study the ions inside of the water potentially through the utilization of liquid chromatography mass spectroscopy to further investigate these ions in the water.

Plant Growth Rate Analysis

The aim of the study is to determine the applicability of our in-house DBD-APPJ as a potential delivery system of nutrients for agriculture, thus understanding the effect of PAW on vegetable plants is necessary. As previously mentioned, the plants utilized for the investigation include *Raphanus sativus* (radish), *Capsicum frutescens* (hot pepper), *capsicum annuum* (sweet pepper), and *solanum lycopersicum* (tomato). Each plant was studied for a period of 60 days and watered everyday with approximately 25 mL of either tap or PAW. Figure (23) shows the overall resulting plant growth for a period of 60 days. The pots are organized in such a way that each plant may be identified the same in the entire image, in other words, at the top of the image the pots are organized as such; top left is tomato, top right is hot pepper, bottom left is sweet pepper, and bottom right is radish. This is true for all the images shown.

Figure 23.Plant growth rate comparison of 15, 30, 45, and 60 days respectively (top to bottom).

It is apparent that PAW played a role in increasing the growth rate of all plants as the 60 days are reached. The control set up which is the first column in the image resulted in a gradual growth through the 60 days for all

seeds planted. As the PAW treatment time was increased there is a dramatic increase in growth rate, in this case growth rate is defined as both the length of the stem and the number of leaves each plant produces as a function of passing time. Figure (24) shows the differences in the number of leaves for each type of plant produced during the 60 days for tap water and PAW. While Figure (25) illustrates the growth rate of the stem during the same allotted time.

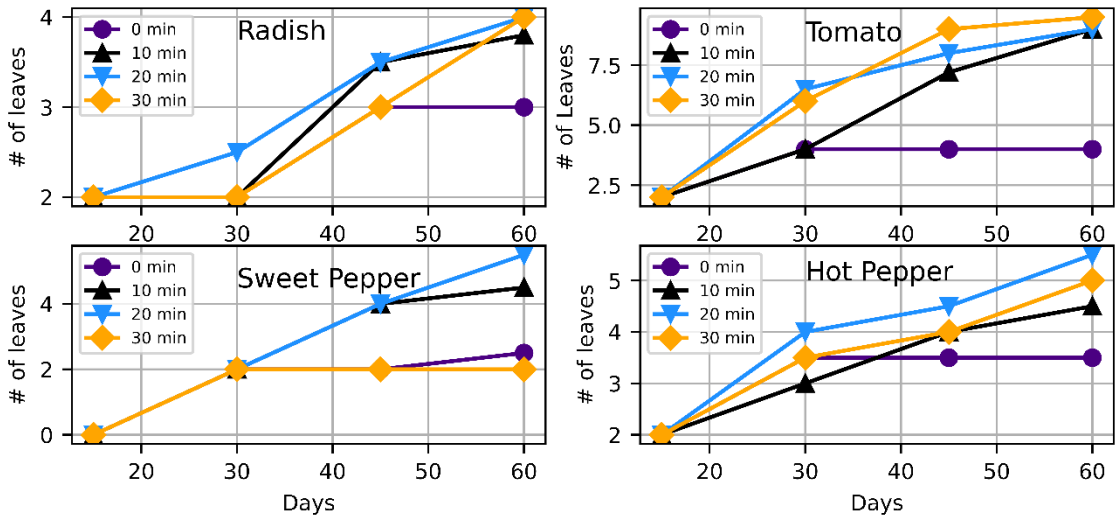

Figure 24.Growth rate of leaves for both tap water and PAW during a 60-day growth period.

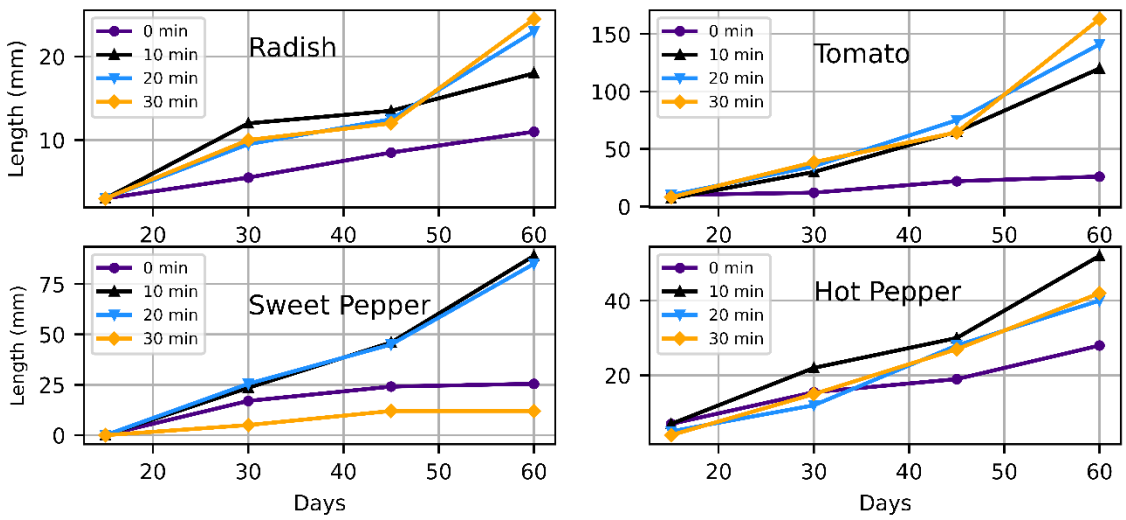

Figure 25.Growth rate of stem for both tap water and PAW during a 60-day growth period.

The results indicate that there is a significant increase in both the number of leaves and the stem length for each kind of plant. This is a result of increase NO_3^- from plasma interaction with air, water surface, and other aqueous reactions occurring during treatment time. When plants receive an appropriate amount of nitrate, it can stimulate the production of chlorophyll, which is crucial to photosynthesis, this in turn promotes leaf growth, leading to an increased number of leaves [109]. For all cases, the tap water samples did not increase in the number of leaves, which resulted from the fact that the nitrate remained constant throughout the 60-day study. An interesting observation of leaf count is the sweet pepper with 30 min PAW, it remained constant for the entirety of the study. The acidity due to the increase in H^+ produced by the plasma increases dramatically thus decreasing the pH< 3 which is acidic for pepper plants [110]. The tomato plants exhibited a

behavior relatively different than the other plants, though its preferred pH for healthy growth lies between 6.2-6.8, it is apparent that the acidity of the water still increase the growth of the number of leaves. While there is plenty of lush relative to other plants, it is possible for the tomato plants to exhibit an increase in vigorous foliage and have little fruit production. The plasma treatment of 20- and 30-min PAW seems to have the highest yield in leaves for all plants, except sweet pepper which had 10 min PAW.

The same effect of PAW was observed for stem length, unlike leaves when stems receive adequate nitrate, it promotes cell division and elongation in plant stems. When the plants receive sufficient nitrate, their stems are likely to grow longer and stronger [111]. In addition to NO_3^-, the DBD-APPJ plasma also introduces H_2O_2 as one of the potential products during ignition, and thus in the case of the stem length being affected there may be more than one source of growth enhancement from both of these chemical species generated in the PAW. Unlike number of leaves, which had a gradual increase in the number of leaves observed per unit time, the stem had an increase that began as gradual for most plants, but after 45-day period there seems to be a increase in steepness in the growth of the plants that were water with PAW. The control samples watered with tap water on the other hand, had a constant stem rate of elongation for all plants, and like the

leaves the sweet pepper plant may have been affected by the increase in acidity of the PAW during plasma treatment. Tomato, radish and sweet pepper saw an almost doubling in length from day 45 to day 60, an indication that under a controlled environment and consistent watering plants can exhibit an increase in stem length when utilizing PAW.

Conclusion:

An atmospheric pressure plasma jet with dielectric barrier discharge configuration was investigated and applied for application in agriculture application of growing vegetable plants. The reactor parameters such as pressure, flow rate, and power remained constant for the duration of the study and plants grown were observed and water for a period of 60 days. The plants that were used for the investigation included: Raphanus sativus (radish), Capsicum frutescens (hot pepper), capsicum annuum (sweet pepper), and solanum lycopersicum (tomato). Results indicate that the rate of growth of plants which was categorized as the increase in number of leaves grown during a 60-day period increased for most of the plants except those not grown with PAW. Furthermore, radish and sweet pepper did not exhibit similar growth as the other plants, which may be due to the acidity of the PAW due to the increase in H^+ ions in the water or the excited N_2 nitrogen molecules oxidized during ignition causing an increase in nitrate through

various reactions. The stem length was also studied to determine if there was a change in growth rate as a function of treatment time for all plants. The results showed that the DBD-APPJ could increase the growth rate of each plant by at least 3 times that of tap water watered plants. The nitrate measured post treatment resulted in an increase in both stem length growth rate and an increase in the number of leaves. Lastly, the N_2 ($C^3\Pi_u \rightarrow B^3\Pi_g$) was observed in capture spectra utilizing optical emission spectroscopy which gave an indication of the ionization potential of the reactor. The rotational and vibrational temperatures are indicative of an increased number of N_2 excited molecules that could be measured via nitrate ion measurements. Overall, the in-house DBD-APPJ has a potential to serve as an alternative to current methods of agriculture and a more in-depth study with statistical analysis is necessary to obtain better data for plant growth rate.

References:

1) Fridman A, Kennedy LA. Plasma physics and engineering. CRC press; 2004.
2) Chu PK, Lu X. Low Temperature Plasma Technology: Methods and Applications. CRC Press; 2013. 493 p.
3) Becker KH, Kogelschatz U, Schoenbach KH, Barker RJ. Non-equilibrium air plasmas at atmospheric pressure. CRC press; 2004.
4) Holub M. On the measurement of plasma power in atmospheric pressure DBD plasma reactors. Int J Appl Electromagnet Mech. 2012 Sep 5;39(1-4):81–7.
5) Walsh JL, Kong MG. Contrasting characteristics of linear-field and cross-field atmospheric plasma jets. Appl Phys Lett. 2008;93. Available: https://pubs.aip.org/aip/apl/article-abstract/93/11/111501/335692
6) Lu X, Laroussi M, Puech V. On atmospheric-pressure non-equilibrium plasma jets and plasma bullets. Plasma Sources Sci Technol. 2012;21: 034005.
7) Rajasekaran P, Mertmann P, Bibinov N, Wandke D, Viöl W, Awakowicz P. Filamentary and homogeneous modes of dielectric barrier discharge (DBD) in air: Investigation through plasma characterization and simulation of surface irradiation. Plasma Process Polym. 2010 Aug 23;7(8):665–75.

8) MDPI. Cold Plasma: Characteristics and Applications in Medicine. MDPI; 2021.

9) Sarani A, Nikiforov AY, Leys C. Atmospheric pressure plasma jet in Ar and Ar/H2O mixtures: Optical emission spectroscopy and temperature measurements. Phys Plasmas. 2010;17: 063504.

10) Gottschalk C, Libra JA, Saupe A. Ozonation of Water and Waste Water: A Practical Guide to Understanding Ozone and its Applications. John Wiley & Sons; 2009.

11) Radzig AA, Smirnov BM. Reference Data on Atoms, Molecules, and Ions. Springer Science & Business Media; 2012.

12) Becker KH, Kogelschatz U, Schoenbach KH, Barker RJ. Non-equilibrium air plasmas at atmospheric pressure. CRC press; 2004.

13) Fujimoto T. Plasma Spectroscopy. In: Fujimoto T, Iwamae A, editors. Plasma Polarization Spectroscopy. Berlin, Heidelberg: Springer Berlin Heidelberg; 2008. pp. 29–49.

14) Kunze H-J. Introduction to Plasma Spectroscopy. Springer Science & Business Media; 2009.

15) Misra NN, Schlüter O, Cullen PJ. Cold Plasma in Food and Agriculture: Fundamentals and Applications. Academic Press; 2016.

16) Pankaj SK, Bueno-Ferrer C, O'Neill L, Tiwari BK, Bourke P, Cullen PJ. Characterization of dielectric barrier discharge atmospheric air

plasma treated chitosan films. J Food Process Preserv. 2017 Feb;41(1):e12889.

17) Ceriani E, Marotta E, Shapoval V, Favaro G, Paradisi C. Complete mineralization of organic pollutants in water by treatment with air non-thermal plasma. Chem Eng J. 2018 Apr 1;337:567–75.

18) Jiang J, 蒋佳峰, He X, 何昕., Li L, 李玲., et al. Effect of Cold Plasma Treatment on Seed Germination and Growth of Wheat. Plasma Sci Technol. 2014 Jan 1;16(1):54.

19) Šerá B, Gajdovâ I, Černâk M, Gavril B, Hnatiuc E, Kováčik D, et al. How various plasma sources may affect seed germination and growth. 2012 13th International Conference on Optimization of Electrical and Electronic Equipment (OPTIM). 2012. pp. 1365–1370.

20) Volin JC, Denes FS, Young RA, Park SMT. Modification of seed germination performance through cold plasma chemistry technology. Crop Sci. 2000 Nov;40(6):1706–18.

21) Nani L, Tampieri F, Ceriani E, Marotta E, Paradisi C. ROS production and removal of the herbicide metolachlor by air non-thermal plasma produced by DBD, DC− and DC+ discharges implemented within the same reactor. J Phys D Appl Phys. 2018 Jun 13;51(27):274002.

22) Burlica R, Kirkpatrick MJ, Locke BR. Formation of reactive species in gliding arc discharges with liquid water. J Electrostat. 2006 Jan;64(1):35–43.

23) Ranieri P, Sponsel N, Kizer J, Rojas-Pierce M, Hernández R, Gatiboni L, et al. Plasma agriculture: Review from the perspective of the plant and its ecosystem. Plasma Process Polym. 2021 Jan;18(1):2000162.

24) Fridman A. Plasma Chemistry. Cambridge University Press; 2008. 1025 p.

25) ation)

26) Coskun, D. et al. (2017) 'Nitrogen transformations in modern agriculture and the role of biological nitrification inhibition', Nature plants, 3, p. 17074.

27) Ranieri, P. et al. (2021) 'Plasma agriculture: Review from the perspective of the plant and its ecosystem', Plasma processes and polymers , 18(1), p. 2000162.

28) Bindraban, P.S. et al. (2020) 'Safeguarding human and planetary health demands a fertilizer sector transformation', PLANTS, PEOPLE, PLANET, 2(4), pp. 302–309.

29) Linquist, B.A. et al. (2012) 'Fertilizer management practices and greenhouse gas emissions from rice systems: A quantitative review and analysis', Field crops research, 135, pp. 10–21.

30) Xia, Y. et al. (2020) 'Recent advances in control technologies for non-point source pollution with nitrogen and phosphorous from agricultural runoff: current practices and future prospects', Applied Biological Chemistry, 63(1), pp. 1–13.

31) Billen, G., Garnier, J. and Lassaletta, L. (2013) 'The nitrogen cascade from agricultural soils to the sea: modelling nitrogen transfers at regional watershed and global scales', Philosophical transactions of the Royal Society of London. Series B, Biological sciences, 368(1621), p. 20130123.

32) NOAA. What is eutrophication? National Ocean Service website, https://oceanservice.noaa.gov/facts/eutrophication.html, 10/05/17.

33) NOAA. Historical Maps and Charts audio podcast. National Ocean Service website, https://oceanservice.noaa.gov/podcast/july17/nop08-historical-maps-charts.html, accessed on 8/13/17.

34) Buendia, J.A., Perez-Lopez, E. and Venkattraman, A. (2018) 'System-level model and experiments for irrigation water alkalinity reduction and enrichment using an atmospheric pressure dielectric barrier discharge', Water research, 144, pp. 728–739.

35) Plotnikov, V., Diaz, G. and Leal-Quiros, E. (2017) 'Elevated Concentration of Nitrate Ions in Water Through Direct Treatment by Dielectric Barrier Discharge', IEEE transactions on plasma science. IEEE Nuclear and Plasma Sciences Society, 45(12), pp. 3246–3251.

36) Sivachandiran, L. and Khacef, A. (2017) 'Enhanced seed germination and plant growth by atmospheric pressure cold air plasma: combined effect of seed and water treatment', RSC advances, 7(4), pp. 1822–1832.

37)Volin, J.C. et al. (2000) 'Modification of seed germination performance through cold plasma chemistry technology', Crop science, 40(6), pp. 1706–1718.

38)Jiang, J. et al. (2014) 'Effect of Cold Plasma Treatment on Seed Germination and Growth of Wheat', Plasma Science and Technology, 16(1), p. 54.

39)Gao, X. et al. (2019) 'Effect of Dielectric Barrier Discharge Cold Plasma on Pea Seed Growth', Journal of agricultural and food chemistry, 67(39), pp. 10813–10822.

40)Yoon, S.-Y. et al. (2018) 'Mutual Interaction between Plasma Characteristics and Liquid Properties in AC-driven Pin-to-Liquid Discharge', Scientific reports, 8(1), p. 12037.

41)Lee, S.H. et al. (2011) 'Efficacy of a new navigable percutaneous disc decompression device (L'DISQ) in patients with herniated nucleus pulposus related to radicular pain', Pain medicine , 12(3), pp. 370–376.

42)Jung, S. et al. (2015) 'The use of atmospheric pressure plasma-treated water as a source of nitrite for emulsion-type sausage', Meat science, 108, pp. 132–137.

43)Foster, J.E. (2017) 'Plasma-based water purification: Challenges and prospects for the future', Physics of plasmas, 24(5), p. 055501.

44) Subramanian, P.S.G. et al. (2021) 'Plasma-activated water from DBD as a source of nitrogen for agriculture: Specific energy and stability studies', Journal of applied physics, 129(9), p. 093303.

45) Judée, F. et al. (2018) 'Plasma-activation of tap water using DBD for agronomy applications: Identification and quantification of long lifetime chemical species and production/consumption mechanisms', Water research, 133, pp. 47–59.

46) Tian, W. and Kushner, M.J. (2014) 'Atmospheric pressure dielectric barrier discharges interacting with liquid covered tissue', Journal of physics D: Applied physics, 47(16), p. 165201.

47) Bradu, C. et al. (2020) 'Reactive nitrogen species in plasma-activated water: generation, chemistry and application in agriculture', Journal of physics D: Applied physics, 53(22), p. 223001.

48) Lu, X. et al. (2016) 'Reactive species in non-equilibrium atmospheric-pressure plasmas: Generation, transport, and biological effects', Physics reports, 630, pp. 1–84.

49) Nishime, T.M.C. et al. (2020) 'A Coaxial Dielectric Barrier Discharge Reactor for Treatment of Winter Wheat Seeds', NATO Advanced Science Institutes series E: Applied sciences, 10(20), p. 7133.

50) Sivachandiran, L. and Khacef, A. (2017) 'Enhanced seed germination and plant growth by atmospheric pressure cold air plasma: combined

effect of seed and water treatment', RSC advances, 7(4), pp. 1822–1832.

51) Švubová, R. et al. (2021) 'Evaluation of the Impact of Cold Atmospheric Pressure Plasma on Soybean Seed Germination', Plants, 10(1). doi:10.3390/plants10010177.

52) Degutytė-Fomins, L. et al. (2020) 'Relationship between cold plasma treatment-induced changes in radish seed germination and phytohormone balance', Japanese journal of applied physics, 59(SH), p. SH1001.

53) Li, R. et al. (2016) 'Study on remediation of phenanthrene contaminated soil by pulsed dielectric barrier discharge plasma: The role of active species', Chemical engineering journal , 296, pp. 132–140.

54) Liu, H. et al. (2021) 'Effect of non-thermal plasma on carbon dioxide reforming of methane to hydrogen', Proceedings of the Institution of Civil Engineers - Energy, 174(2), pp. 67–78.

55) Cheng, D.-G. et al. (2006) 'Carbon dioxide reforming of methane over Ni/Al2O3 treated with glow discharge plasma', Catalysis Today, 115(1), pp. 205–210.

56) Yoon, S.-Y. et al. (2018) 'Mutual Interaction between Plasma Characteristics and Liquid Properties in AC-driven Pin-to-Liquid Discharge', Scientific reports, 8(1), p. 12037.

57) Chu, P.K. and Lu, X. (2013) Low Temperature Plasma Technology: Methods and Applications. CRC Press.

58) Van Gaens, W. and Bogaerts, A. (2014) 'Corrigendum: Kinetic modelling for an atmospheric pressure argon plasma jet in humid air (2013 J. Phys. D: Appl. Phys. 46 275201)', Journal of Physics D: Applied Physics, p. 079502. doi:10.1088/0022-3727/47/7/079502.

59) Tian, W. and Kushner, M.J. (2014) 'Atmospheric pressure dielectric barrier discharges interacting with liquid covered tissue', Journal of physics D: Applied physics, 47(16), p. 165201.

60) Zaplotnik, R., Bišćan, M., Kregar, Z., Cvelbar, U., Mozetič, M., & Milošević, S. (2015). Influence of a sample surface on single electrode atmospheric plasma jet parameters. Spectrochimica Acta. Part B: Atomic Spectroscopy, 103-104, 124–130.

61) Attri, P., Yusupov, M., Park, J. H., Lingamdinne, L. P., Koduru, J. R., Shiratani, M., Choi, E. H., & Bogaerts, A. (2016). Mechanism and comparison of needle-type non-thermal direct and indirect atmospheric pressure plasma jets on the degradation of dyes. Scientific Reports, 6, 34419.

62) Foster, J., Sommers, B. S., Gucker, S. N., Blankson, I. M., & Adamovsky, G. (2012). Perspectives on the Interaction of Plasmas With Liquid Water for Water Purification. IEEE Transactions on Plasma Science. IEEE Nuclear and Plasma Sciences Society, 40(5), 1311–1323.

63) Ser., J. P. :. (n.d.). Experimental investigation of Lissajous figure shapes in planar and surface dielectric barrier discharges. https://iopscience.iop.org/article/10.1088/1742-6596/550/1/012039/pdf

64) Holub, M. (2012). On the measurement of plasma power in atmospheric pressure DBD plasma reactors. International Journal of Applied Electromagnetics and Mechanics, 39(1-4), 81–87.

65) Hao, Z., Ji, S., Liu, H., & Song, Y. (2014). Effect of the grounded electrode on cold ar atmospheric pressure plasma jet generated with a simple DBD configuration. IEEE Transactions on Plasma Science. IEEE Nuclear and Plasma Sciences Society, 42(3), 824–832.

66) Tao, X., Rongde, L. U., & Li, H. (2012). Electrical Characteristics of Dielectric-Barrier Discharges in Atmospheric Pressure Air Using a Power-Frequency Voltage Source *. Plasma Science and Technology, 14(8). https://doi.org/10.1088/1009-0630/14/8/08

67) United Nations. 2023. World Population Day 2023: The Day of Eight Billion. United Nations Department of Economic and Social Affairs. URL: https://www.un.org/development/desa/pd/events/day-eight-billion

68) Food and Agriculture Organization (FAO). 2023. Climate Change and Food Security - Chapter 3: Impact of climate change on fisheries and aquaculture. Food and Agriculture Organization (FAO) of the United Nations. URL: https://www.fao.org/3/cc2211en/online/cc2211en.html#chapter-3

69) Sabzevari S, Hofman J. A worldwide review of currently used pesticides' monitoring in agricultural soils. Sci Total Environ. 2022;812: 152344.

70) Wu G, Fan Y, Riaz N. Spatial Analysis of Agriculture Ecological Efficiency and Its Influence on Fiscal Expenditures. Sustain Sci Pract Policy. 2022;14: 9994.

71) Sargent RD, Carrillo J, Kremen C. Common pesticides disrupt critical ecological interactions. Trends Ecol Evol. 2023;38: 207–210.

72) Chrustek A, Hołyńska-Iwan I, Dziembowska I, Bogusiewicz J, Wróblewski M, Cwynar A, et al. Current Research on the Safety of Pyrethroids Used as Insecticides. Medicina. 2018;54. doi:10.3390/medicina54040061

73) Elser BA, Hing B, Stevens HE. A narrative review of converging evidence addressing developmental toxicity of pyrethroid insecticides. Crit Rev Toxicol. 2022;52: 371–388.

74) Bora K. Spatial patterns of fertilizer use and imbalances: Evidence from rice cultivation in India. Environmental Challenges. 2022;7: 100452.

75) Jin Q, Wang C, Sardans J, Vancov T, Fang Y, Wu L, et al. Effect of soil degradation on the carbon concentration and retention of nitrogen and phosphorus across Chinese rice paddy fields. Catena. 2022;209: 105810.

76) Bhatt MK, Labanya R, Joshi HC. Influence of Long-term Chemical fertilizers and Organic Manures on Soil Fertility -A Review. Universal Journal of Agricultural Research. 2019;7: 177–188.

77) Guo D, Liu H, Zhou L, Xie J, He C. Plasma-activated water production and its application in agriculture. J Sci Food Agric. 2021;101: 4891–4899.

78) Kim J-W, Puligundla P, Mok C. Microbial decontamination of dried laver using corona discharge plasma jet (CDPJ). J Food Eng. 2015;161: 24–32.

79) Feng X, Ma X, Liu H, Xie J, He C, Fan R. Argon plasma effects on maize: pesticide degradation and quality changes. J Sci Food Agric. 2019;99: 5491–5498.

80) Iqbal T, Farooq M, Afsheen S, Abrar M, Yousaf M, Ijaz M. Cold plasma treatment and laser irradiation of Triticum spp. seeds for sterilization and germination. J Laser Appl. 2019;31. Available: https://pubs.aip.org/lia/jla/article/31/4/042013/222393

81) Ranieri P, Sponsel N, Kizer J, Rojas-Pierce M, Hernández R, Gatiboni L, et al. Plasma agriculture: Review from the perspective of the plant and its ecosystem. Plasma Process Polym. 2021;18: 2000162.

82) Gucker SN, Sommers BS, Foster JE. Plasma Production in Isolated Bubbles. IEEE Trans Plasma Sci IEEE Nucl Plasma Sci Soc. 2014;42: 2636–2637.

83) Kondeti VSS, Bruggeman PJ. The interaction of an atmospheric pressure plasma jet with liquid water: dimple dynamics and its impact on crystal violet decomposition. J Phys D Appl Phys. 2020;54: 045204.

84) Gott RP, Engeling KW, Olson J, Franco C. Plasma activated water: a study of gas type, electrode material, and power supply selection and the impact on the final frontier. Phys Chem Chem Phys. 2023;25: 5130–5145.

85) Xiang Q, Fan L, Li Y, Dong S, Li K, Bai Y. A review on recent advances in plasma-activated water for food safety: current applications and future trends. Crit Rev Food Sci Nutr. 2022;62: 2250–2268.

86) Samukawa S, Hori M, Rauf S, Tachibana K, Bruggeman P, Kroesen G, et al. The 2012 Plasma Roadmap. J Phys D Appl Phys. 2012;45: 253001.

87) Thirumdas R, Kothakota A, Annapure U, Siliveru K, Blundell R, Gatt R, et al. Plasma activated water (PAW): Chemistry, physico-chemical properties, applications in food and agriculture. Trends Food Sci Technol. 2018;77: 21–31.

88) Jin YS, Cho C, Kim D, Sohn CH, Ha C-S, Han S-T. Mass production of plasma activated water by an atmospheric pressure plasma. Jpn J Appl Phys. 2020;59: SHHF05.

89) Domonkos M, Tichá P, Trejbal J, Demo P. Applications of Cold Atmospheric Pressure Plasma Technology in Medicine, Agriculture and Food Industry. NATO Adv Sci Inst Ser E Appl Sci. 2021;11: 4809.

90) Stryczewska HD, Boiko O. Applications of Plasma Produced with Electrical Discharges in Gases for Agriculture and Biomedicine. NATO Adv Sci Inst Ser E Appl Sci. 2022;12: 4405.

91) Hoeben WFLM, van Ooij PP, Schram DC, Huiskamp T, Pemen AJM, Lukeš P. On the Possibilities of Straightforward Characterization of Plasma Activated Water. Plasma Chem Plasma Process. 2019;39: 597–626.

92) Sarinont T, Katayama R, Wada Y, Koga K, Shiratani M. Plant Growth Enhancement of Seeds Immersed in Plasma Activated Water. MRS Advances. 2017;2: 995–1000.

93) Fan L, Liu X, Ma Y, Xiang Q. Effects of plasma-activated water treatment on seed germination and growth of mung bean sprouts. Journal of Taibah University for Science. 2020;14: 823–830.

94) City Of Merced Consumer Confidence Report Reporting Year 2022.

95) Karakas E, Laroussi M. Experimental studies on the plasma bullet propagation and its inhibition. J Appl Phys. 2010. Available: https://pubs.aip.org/aip/jap/article-abstract/108/6/063305/348715

96) Sands BL, Ganguly BN, Tachibana K. A streamer-like atmospheric pressure plasma jet. Appl Phys Lett. 2008;92. Available: https://pubs.aip.org/aip/apl/article/92/15/151503/326073

97) Mrotzek J, Viöl W. Spectroscopic Characterization of an Atmospheric Pressure Plasma Jet Used for Cold Plasma Spraying. NATO Adv Sci Inst Ser E Appl Sci. 2022;12: 6814.

98) Hsu Y-W, Yang Y-J, Wu C-Y, Hsu C-C. Downstream Characterization of an Atmospheric Pressure Pulsed Arc Jet. Plasma Chem Plasma Process. 2010;30: 363–372.

99) Zaplotnik R, Primc G, Vesel A. Optical Emission Spectroscopy as a Diagnostic Tool for Characterization of Atmospheric Plasma Jets. NATO Adv Sci Inst Ser E Appl Sci. 2021;11: 2275.

100) Xiao D, Cheng C, Shen J, Lan Y, Xie H, Shu X, et al. Characteristics of atmospheric-pressure non-thermal N2 and N2/O2 gas mixture plasma jet. J Appl Phys. 2014;115: 033303.

101) Voráč J, Kusýn L, Synek P. Deducing rotational quantum-state distributions from overlapping molecular spectra. Rev Sci Instrum. 2019;90: 123102.

102) Voráč J, Synek P, Potočňáková L, Hnilica J, Kudrle V. Batch processing of overlapping molecular spectra as a tool for spatio-temporal diagnostics of power modulated microwave plasma jet. Plasma Sources Sci Technol. 2017;26: 025010.

103) Voráč J, Synek P, Procházka V, Hoder T. State-by-state emission spectra fitting for non-equilibrium plasmas: OH spectra of surface barrier discharge at argon/water interface. J Phys D Appl Phys. 2017;50: 294002.

104) Schutze A, Jeong JY, Babayan SE, Park J, Selwyn GS, Hicks RF. The atmospheric-pressure plasma jet: a review and comparison to other plasma sources. IEEE Trans Plasma Sci IEEE Nucl Plasma Sci Soc. 1998;26: 1685–1694.

105) Javanmard S, Pouryoussefi SG. Comparison of characteristics of atmospheric pressure plasma jets using argon and helium working gases. Curr Appl Phys. 2023;46: 61–69.

106) Huang B, Zhang C, Zhu W, Lu X, Shao T. Ionization waves in nanosecond pulsed atmospheric pressure plasma jets in argon. High Volt Appar. 2021;6: 665–673.

107) Sakakura T, Murakami N, Takatsuji Y, Morimoto M, Haruyama T. Contribution of Discharge Excited Atomic N, N2 *, and N2+ to a Plasma/Liquid Interfacial Reaction as Suggested by Quantitative Analysis. Chemphyschem. 2019;20: 1467–1474.

108) Sarron E, Gadonna-Widehem P, Aussenac T. Ozone Treatments for Preserving Fresh Vegetables Quality: A Critical Review. Foods. 2021;10. doi:10.3390/foods10030605

109) Wang Y, Chen L, Su W, Hao Y, Liu H, Sun G, et al. Effect of Nitrate Concentration on the Growth, Bolting and Related Gene Expression in Flowering Chinese Cabbage. Agronomy. 2021;11: 936.

110) Lee JJ, Neely GE, Perrigan SC, Grothaus LC. Effect of simulated sulfuric acid rain on yield, growth and foliar injury of several crops. Environ Exp Bot. 1981;21: 171–185.

111) Camut L, Gallova B, Jilli L, Sirlin-Josserand M, Carrera E, Sakvarelidze-Achard L, et al. Nitrate signaling promotes plant growth by upregulating gibberellin biosynthesis and destabilization of DELLA proteins. Curr Biol. 2021;31: 4971–4982.e4.

112) Brandenburg R, Bogaerts A, Bongers W, Fridman A, Fridman G, Locke BR, et al. White paper on the future of plasma science in environment, for gas conversion and agriculture. Plasma Process Polym. 2019;16: 1700238.

113) Kawai Y, Ikegami H, Sato N, Matsuda A, Uchino K, Kuzuya M, et al. Industrial Plasma Technology: Applications from Environmental to Energy Technologies. John Wiley & Sons; 2010.

114) Yoa S-J, Cho Y-S, Choi Y-S, Baek J-H. Characteristics of electrostatic cyclone/bag filter with inlet types (lab and pilot scale). Korean J Chem Eng. 2001;18: 539–546.

115) Penetrante BM, Schultheis SE, North Atlantic Treaty Organization. Scientific Affairs Division. Non-thermal Plasma

Techniques for Pollution Control: Electron beam and electrical discharge processing. Springer-Verlag; 1993.

116) Darmawan A, Aziz M, Ajiwibowo MW, Biddinika MK, Tokimatsu K, Lokahita B. Chapter 5 - Integrated ammonia production from the empty fruit bunch. In: Darmawan A, Aziz M, editors. Innovative Energy Conversion from Biomass Waste. Elsevier; 2022. pp. 149–185.

117) Haber F, van Oordt G. Über die Bildung von Ammoniak den Elementen. Z Anorg Allg Chem. 1905;44: 341–378.

118) Schlögl DR. Part B 2.1. Ammonia Synthesis. [cited 16 Aug 2023].Available https://pure.mpg.de/rest/items/item_736938/component/file_932945/content

119) Miyamoto S, Ryan J, Stroehlein JL. Potentially beneficial uses of sulfuric acid in southwestern agriculture. J Environ Qual. 1975;4: 431–437.

120) Martin C, Alriksson B, Sjöde A, Nilvebrant N-O, Jönsson LJ. Dilute Sulfuric Acid Pretreatment of Agricultural and Agro-Industrial Residues for Ethanol Production. In: Mielenz JR, Klasson KT, Adney WS, McMillan JD, editors. Applied Biochemistry and Biotecnology: The Twenty-Eighth Symposium Proceedings of the Twenty-Eight Symposium on Biotechnology for Fuels and Chemicals Held April 30–

May 3, 2006, in Nashville, Tennessee. Totowa, NJ: Humana Press; 2007. pp. 339–352.

121) Lucheta AR, Lambais MR. Sulfur in agriculture. Rev Bras Cienc Solo. 2012;36: 1369–1379.

122) Wang Y, Li T, Yu Y, Zhang B. Electrochemical synthesis of nitric acid from nitrogen oxidation. Angew Chem Weinheim Bergstr Ger. 2022;134. doi:10.1002/ange.202115409

123) Bussink DW, Huijsmans JFM, Ketelaars JJM. Ammonia volatilization from nitric-acid-treated cattle slurry surface applied to grassland. NJAS. 1994;42: 293–309.

124) Hunt LB. The Ammonia Oxidation Process for Nitric Acid Manufacture. Platin Met Rev. 1958;2: 129–134.